ANALYSIS OF THE F-CORONA ACCORDING TO THE MIE THEORY

PART I

Mathematical Formulation And Uniqueness of the Derived Theoretical Models

December 18, 1965

Prepared for

NATIONAL AERONAUTICS AND SPACE ADMINISTRATION

NASA Contract NASW-1206

Prepared by

R. S. Powell and R. R. Circle

Space Systems Laboratory

MELPAR, INC.

7700 Arlington Boulevard

Falls Church, Virginia

ANALYSIS OF THE F-CORONA ACCORDING TO THE MIE THEORY

PART I

Mathematical Formulation and Uniqueness of the Derived Theoretical Models

Prepared by

R. S. Powell and R. R. Circle
Space Systems Laboratory

Melpar, Inc.
7700 Arlington Boulevard
Falls Church, Virginia

December 18, 1965

Prepared for

National Aeronautics and Space Administration
Washington, D.C.
NASA Contract NASW-1206

TABLE OF CONTENTS

		Page
	ABSTRACT	4
1.	INTRODUCTION	5
2.	MATHEMATICAL FORMULATION	7
	2.1 Exact Formulation of the Zodiacal Light Problem	7
	2.2 The Cumulative Functions $F(\theta, m, X)$ and $\Delta(\theta, m, X)$	9
	2.3 Simplification of Equations (12) and (17)	21
3.	ANALYTIC METHOD	32
	3.1 Limiting Values of α	33
4.	UNIQUENESS	34
	4.1 Geometrical Ambiguities	34
	4.2 Ambiguities Due to Polydispersion	34
	4.3 Ambiguities Due to Heterogeneity	37
5.	ELECTRONS	39
6.	ACKNOWLEDGMENTS	42
7.	REFERENCES	43

LIST OF ILLUSTRATIONS

Figure		Page
1	Observational Geometry - Zodiacal Light	8
2A	$F(\varepsilon,m,X)$ Refractive Index m = 1.4 (typical)	10
2B	$F(\varepsilon,m,X)$ Refractive Index m = 1.8	11
2C	(ε,m,X) Refractive Index m = 1.51 - 1.632i	12
3	Typical Mathematical Behavior of the Cumulative Brightness Function, F(X), for Various Values of the Scattering Angle, $\theta=\varepsilon$, and Refractive Index, m. (taken from Powell and Donn, 1966) (4 pages)	13
4	Typical Behavior of the Cumulative Polarization Function, p(X) for Various Scattering Angles $\theta=\varepsilon$ and Refractive Indices. (taken from Powell and Donn, 1966) (3 pages)	18
5A	Type 1 Functions, $\Delta(\varepsilon,m,X)$, Characterized by Positive Value and Positive Slope	22
5B	Type 2 Functions, $\Delta(\varepsilon,m,X)$, Characterized by Positive Value With Zero Slope Between 35° and 55°	23
5C	Type 3 Functions, $\Delta(\varepsilon,m,X)$, Characterized by Positive Value With a Negative Slope	24
5D	Type 4 Functions, $\Delta(\varepsilon,m,X)$, Characterized by Negative Slope and Both Positive and Negative Value	25
5E	Type 5 Functions, $\Delta(\varepsilon,m,X)$, Characterized by Negative Values and Zero Slope Between 35° and 65°	26
5F	Type 6 Functions, $\Delta(\varepsilon,m,X)$, Characterized by Oscillatory Shape and Positive and Negative Values	27
6	The Function $S_m(\varepsilon,\alpha)$ Calculated From the Observations of Blackwell and Ingham is Shown for Various Assumed Values of α. $S_m(\varepsilon,\alpha)$ is Defined by Equation 33.	30
7	The Function $T_m(\varepsilon,\alpha)$ Calculated From the Observations of Blackwell and Ingham is Shown for Various Assumed Values of α. $T_m(\varepsilon)$ is Defined by Equation 34.	31
8	Typical Resonance Behavior of the Mie Function $i_j(X)$	36

ABSTRACT

14601

A mathematical model is formulated to remove the integrals over scattering angle and particle size which occur in analyzing observations of the zodiacal light. The resulting algebraic equations are expressed in terms of scattering functions with known and easily recognizable properties. Consequently, the uniqueness of deductions concerning the nature of the interplanetary dust can be determined by studying the mathematical behavior of these functions. In addition, the simplified mathematical formulation allows one to judge the relative value of various observations. Single color observations at elongations in the range $20^{\circ}<\epsilon<70^{\circ}$ give unique information concerning the size distribution of the interplanetary dust but not the chemical composition or electron density. Multi-color observations in this range help in determining the electron density but not the chemical composition. Multi-color observations in the range $110^{\circ}<\epsilon<180^{\circ}$ are most valuable in determining the electron density and chemical composition.

It is shown that the radial decay constant, α, must be less than 1.5.

Author

1. INTRODUCTION

From observations of the brightness and polarization of the zodiacal light as a function of the elongation, ϵ, it is possible, in principle, to deduce the composition, number density and size of interplanetary particles. Many observations are available, Weinburg (1964) presents an excellent summary, for example. By averaging the measured brightness curves (brightness vs elongation) in the region $\epsilon<90^{\circ}$, one finds a reasonable correlation among results obtained by different observers. However, there is little agreement among these same observers regarding the measured polarization. In addition to observational inconsistencies, the determination of the nature of the zodiacal light is further hampered by analytic difficulties. The mathematical relationships, as derived by Gustov Mie (1908), between the composition and size distribution of the particles on the one hand and the observed polarization and brightness on the other, are very complicated. Various approximations have been applied, but insofar as we know, no one has succeeded in matching the observed polarization curves with exact theoretical curves corresponding to real particles. Since all of the observed polarization curves are different, it would be remarkable if none could be satisfactorily explained by the application of the Mie theory.

The lack of an exact match between the observed polarization and that calculated theoretically from hypothetical models of the interplanetary medium would indicate that many of the observations are wrong, or that the zodiacal light is a more complicated phenomenon than we previously supposed.* It is important to determine which of these alternatives is probable.

Weinberg feels very confident that his observations are accurate.** This confidence is justified when one considers the possibilities for error in the other observations due to wide bandwidth and questionable corrections for the various night sky radiations. His polarization measurements agree somewhat with those of Divari and Krylova (1963), Huruhata (1964), Robley (1962) and Peterson (1961) in the sense that polarization is less than 0.23 for $\epsilon \simeq 70^{\circ}$. On the other hand the observations of Blackwell and Ingham (1961) show very high polarization (P=0.33 at 70°) and agree rather well with those of Elsasser (1963).

---

* For example, Giese and Siedentopf (1962) suggest that the particles may be irregularly shaped and aligned. In that case the Mie Scattering theory, which is only applicable to spherical particles, is not appropriate for analysis of the zodiacal light.

** Personal communication.

Thus, the polarization observations can be roughly divided into two groups; one group represented by the measurements of Weinberg, the other represented by the measurements of Blackwell and Ingham. We assume that either or both are correct.

If neither can be matched by an exact theoretical analysis according to the Mie theory, then the assumption that the zodiacal light results from nearly spherical and unaligned particles is probably wrong. On the other hand, if both can be matched from the Mie theory we must conclude that either: (1) both are accurate and correct indicating that the interplanetary medium changes with time, or (2) the scattering theory can be made to fit nearly any polarization curve.

It was this last possibility which prompted the present study. No information was available regarding the uniqueness of deductions from the Mie theory when the particles are polydisperse.

The possibility that only one observational curve can be theoretically matched would indicate that observations in the other group are grossly in error. In that case, the size distribution, radial distribution and composition of the particles in the interplanetary medium could be determined from the theoretical model used to matched the correct curve. Such a determination would be useful only if the theoretically derived model was unique. Thus, before any further work is done in trying to explain the zodiacal light, it is important to investigate the uniqueness of the mathematical relationships between the measured optical parameters and the parameters representing the physical properties of the particles. These relationships are complicated by the observational geometry of the problem and by the heterogeneous and polydisperse nature of the scatterers. In order to understand the optical contributions from each component in the interplanetary medium, it is necessary to simplify the mathematical formulation so that the measured variables may be expressed in terms of functions with easily recognizable behavior.

In the following volume we present such a mathematical formulation preparatory to a detailed analysis of all observations, and summarize the ambiguities which occur in trying to match the observations with theoretical models. Due to the bulk of numerous graphs required to clarify the mathematical formulations presented herein, the analytic results of all observations will be published separately as part II of this series.

2. MATHEMATICAL FORMULATION

2.1 Exact Formulation of the Zodiacal Light Problem

According to the Mie theory, there is an exact function, $i_j(\varepsilon, m, x)$, which relates the optical character of light scattered by a single spherical particle to its physical properties. The irradiance, I_j, of the light scattered by N particles per cm^3 with radius, a, is given by:

$$dI_j(\theta, \lambda) = \frac{I_o \lambda^2}{8\pi^2 R^2} N(x, \rho)\, i_j(\theta, m, x)\, dv\, dx \qquad (1)$$

where λ is the wavelength, I_o is the spectral irradiance of the illumination at the scattering site distance ρ from the sun, (figure 1), R is the distance from the scattering site to the observer, θ is the scattering angle, m is the refractive index of the particle, and x is the size parameter defined by:

$$x = 2\pi a/\lambda \,. \qquad (2)$$

The small volume, dv, is defined by the intersection of the illuminating beam with the field of view and the subscript, j, indicates the orientation of the electric vector with respect to the scattering plane. The sum of the vertically polarized light (j = 1) and the horizontally polarized light (j = 2) is indicated by neglecting the subscript, i.e.,

$$I = I_1 + I_2 \qquad i = i_1 + i_2 \qquad (3)$$

The irradiance can be expressed interms of the flux of solar radiation, $J_o(\lambda)$, at R_o = 1 A.U.

$$I_o = J_o(\lambda) \frac{R_o^2}{\rho^2} \qquad (4)$$

The size distribution function can be expressed in terms of the size distribution at distance $\rho = R_o$ from the sun:

$$N(x, \rho) = N(x, R_o)\left(\frac{R_o}{\rho}\right)^{\alpha} \qquad (5)$$

where we have assumed that the number density decreases as $\rho^{-\alpha}$. The scattered irradiance is seen coming from a solid angle $\pi \tan^2 \varphi$ where φ

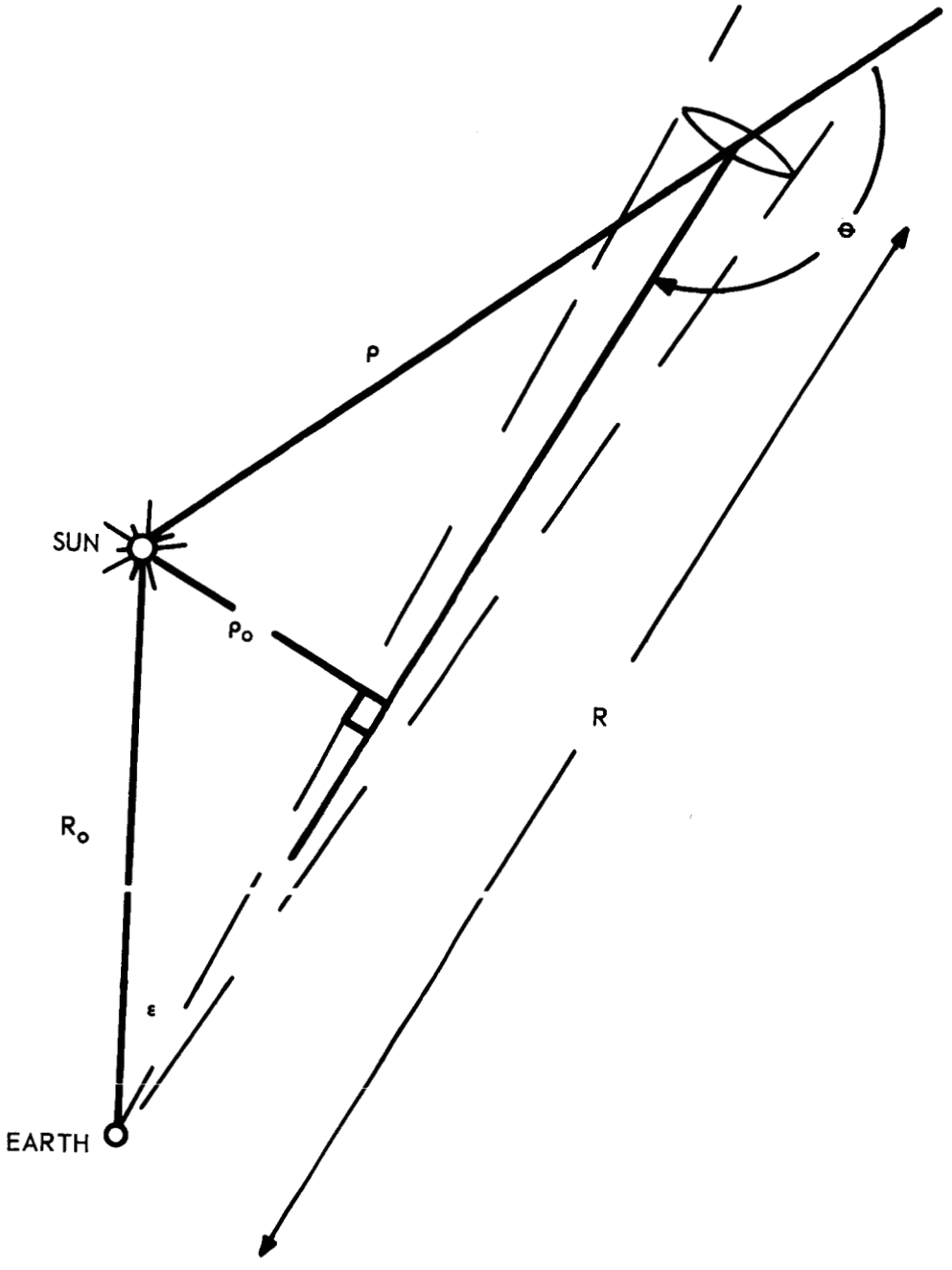

Figure 1. Observational Geometry - Zodiacal Light

is the half angle of the view field. The apparent brightness is therefore:

$$dB_j(\theta, \lambda) = dI_j(\theta, \lambda)/\pi \tan^2 \varphi \qquad (6)$$

The volume increment may be expressed in terms of the scattering angle θ and elongation, ε:

$$dv = R_o \sin\varepsilon \, R^2 \tan^2 \varphi \, d\theta/\sin^2\theta \qquad (7)$$

substituting equations (4) through (7) into equation (1) and integrating over all scattering angles and particle sizes we obtain:

$$B_j(\varepsilon, \lambda) = \frac{J_o(\lambda) R_o}{\sin^{1+\alpha}\varepsilon} \frac{\lambda^2}{8\pi^2} \int_0^{\infty} \int_{\varepsilon}^{\pi} N(x, R_o) \sin^{\alpha}\theta \; i_j(\theta, m, x) \, dx \, d\theta \qquad (8)$$

Equation (8) is exact if the implicit assumptions are reasonable. These assumptions are: 1) the interplanetary dust particles scatter like spheres, 2) the decrease (or increase) in number density with radial distance from the sun is independent of particle size and 3) scattering from electrons is negligible. The latter assumption is certainly not valid for $\varepsilon < 20^o$.

2.2 The Cumulative Functions $F(\theta, m, X)$ and $\Delta(\theta, m, X)$

Consider a uniform distribution of particles containing $\bar{N}(X, R_o)$ particles per cc per increment δx in the range $0 < x < X$. X may be called the termination parameter in the sense that it terminates the unit step function which represents a uniform distribution containing one particle per cc per increment δx.

$$X = \frac{2\pi A}{\lambda} \qquad (9)$$

where A is the radius of the largest particle in the uniform distribution.

The scattering from the terminated unit step distribution of particles is given by:

$$F_j(\theta, m, X) = \int_0^X i_j(\theta, m, x) \, dx \qquad (10)$$

Thus defining the cumulative scattering ratio,* $F_j(\theta, m, X)$. $F(\theta, m, X)$ is presented graphically in figures 2 and 3.

---

* The cumulative scattering ratio was first defined by Donn and Powell (1963).

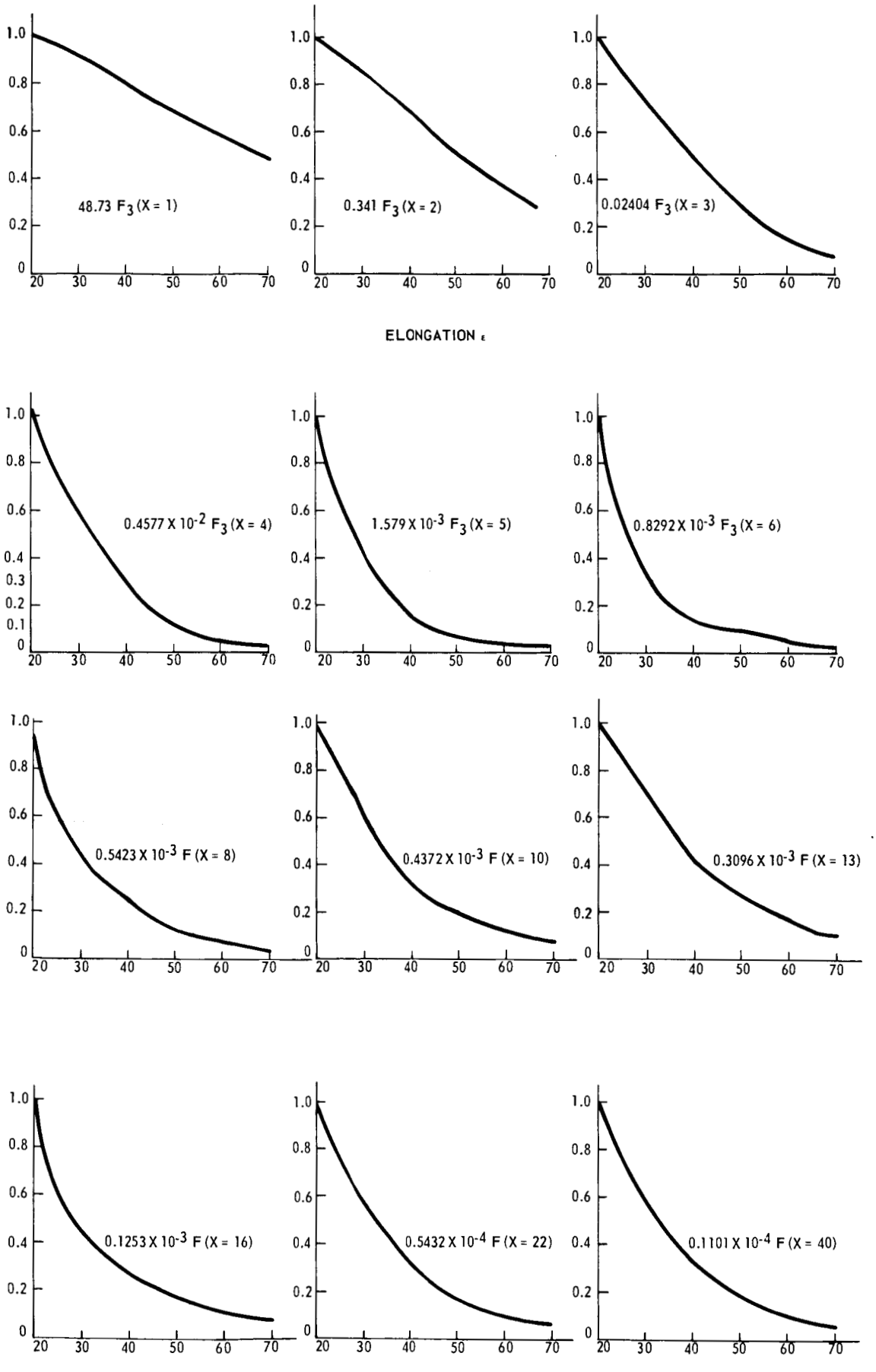

Figure 2A. F(ϵ, m, X) Refractive Index m = 1.4 (typical)

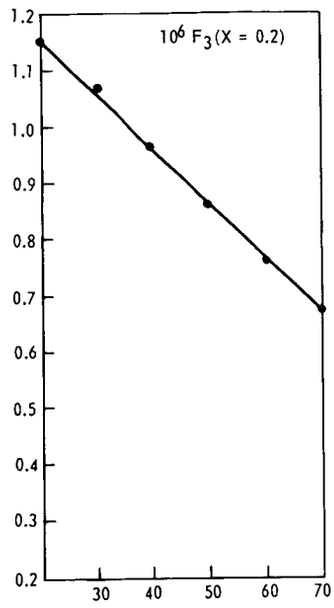
10^6 F_3(X = 0.2)

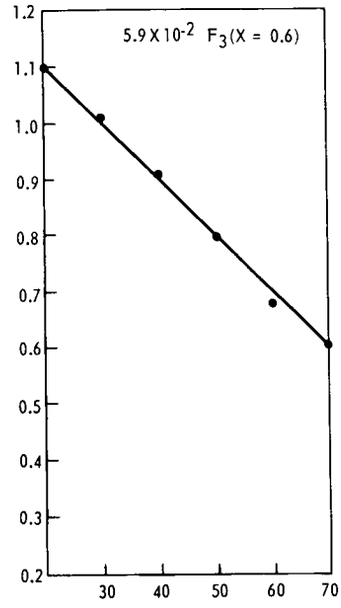
5.9×10^{-2} F_3(X = 0.6)

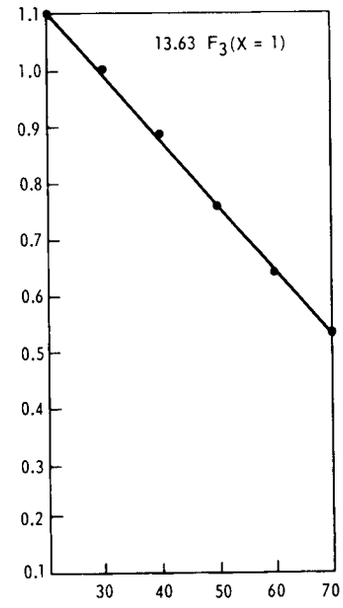
13.63 F_3(X = 1)

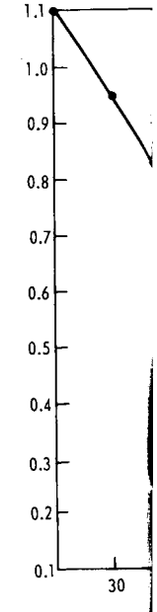

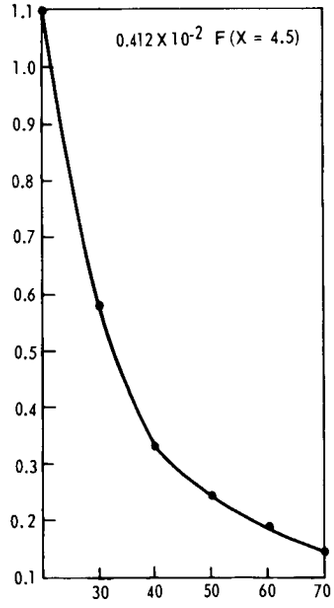
0.412×10^{-2} F(X = 4.5)

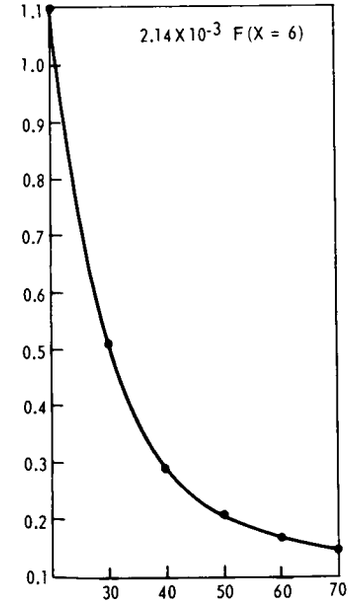
2.14×10^{-3} F(X = 6)

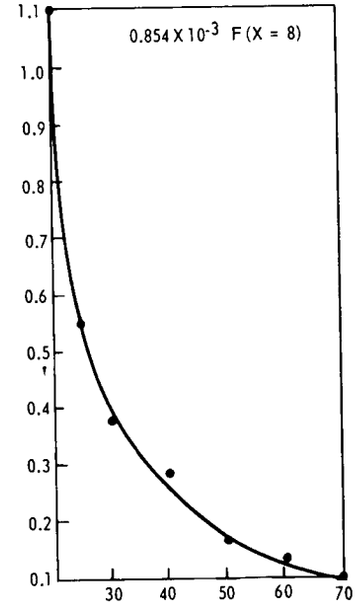
0.854×10^{-3} F(X = 8)

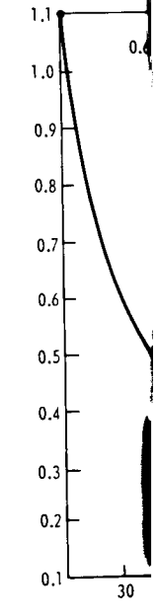

= 1.8

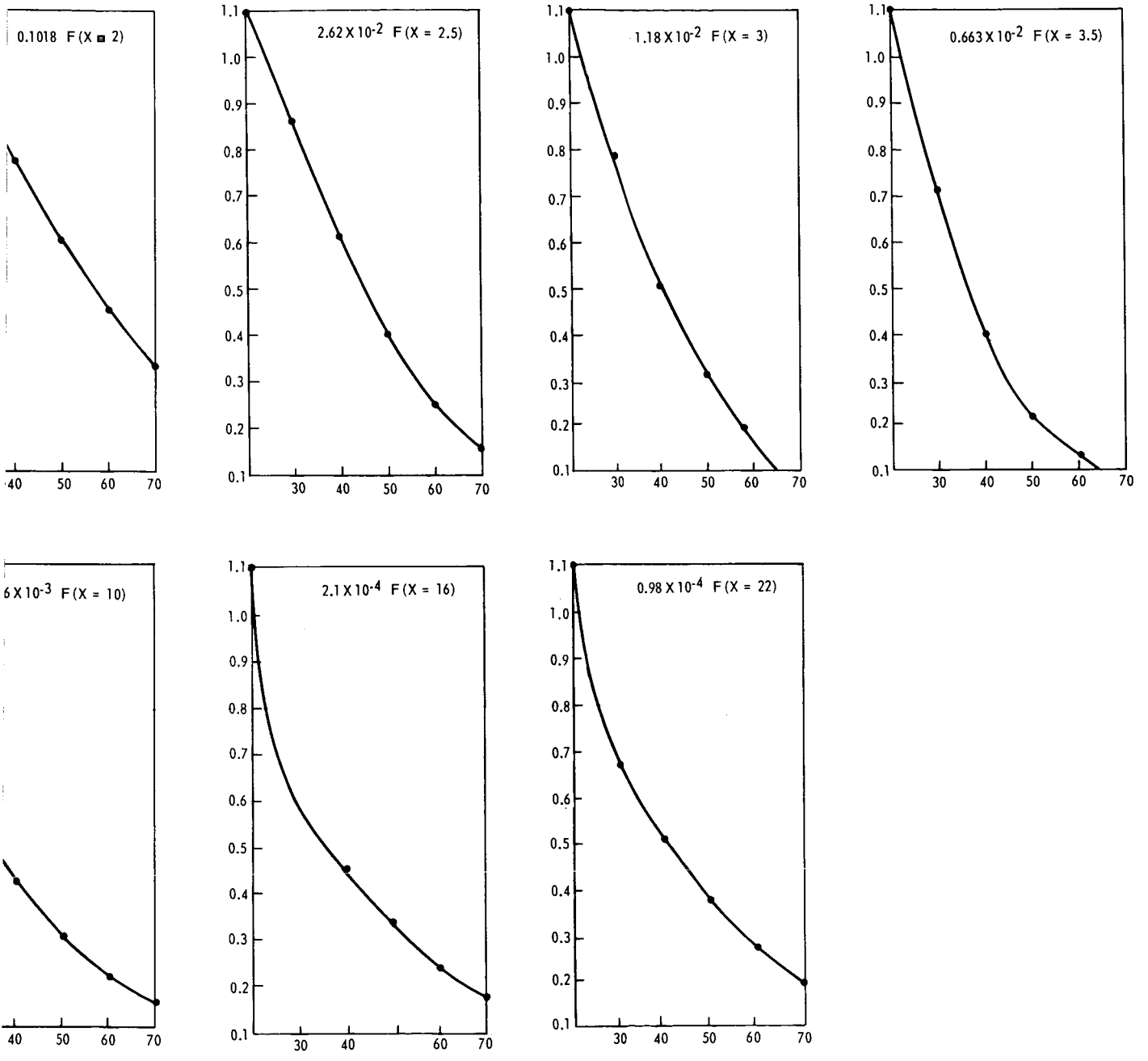

2

Figure 2B. F(∈, m, X) Refractive Index m = 1.8

E4267

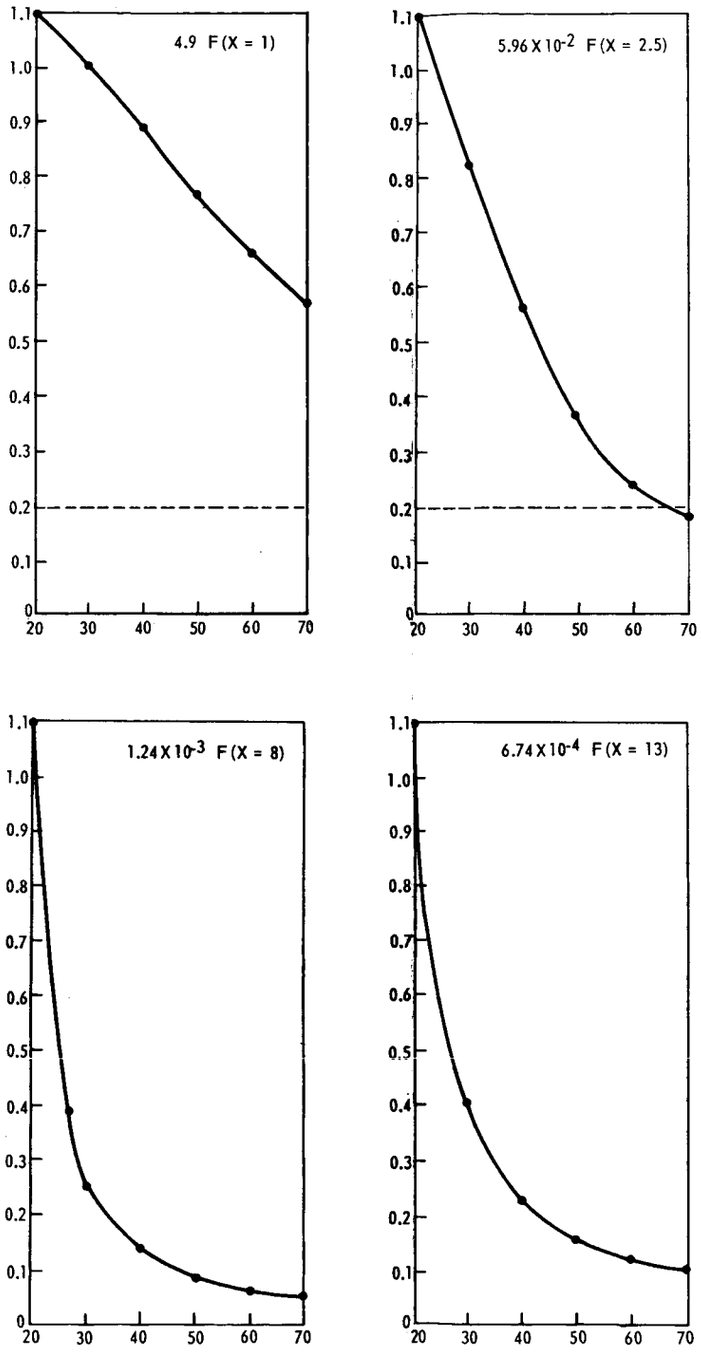
4.9 F(X = 1)
5.96 X 10-2 F(X = 2.5)
1.24 X 10-3 F(X = 8)
6.74 X 10-4 F(X = 13)
1.1
1.0
0.9
0.8
0.7
0.6
0.5
0.4
0.3
0.2
0.1
0
20
30
40
50
60
70

IRON; M = 1.51 - 1.63 i

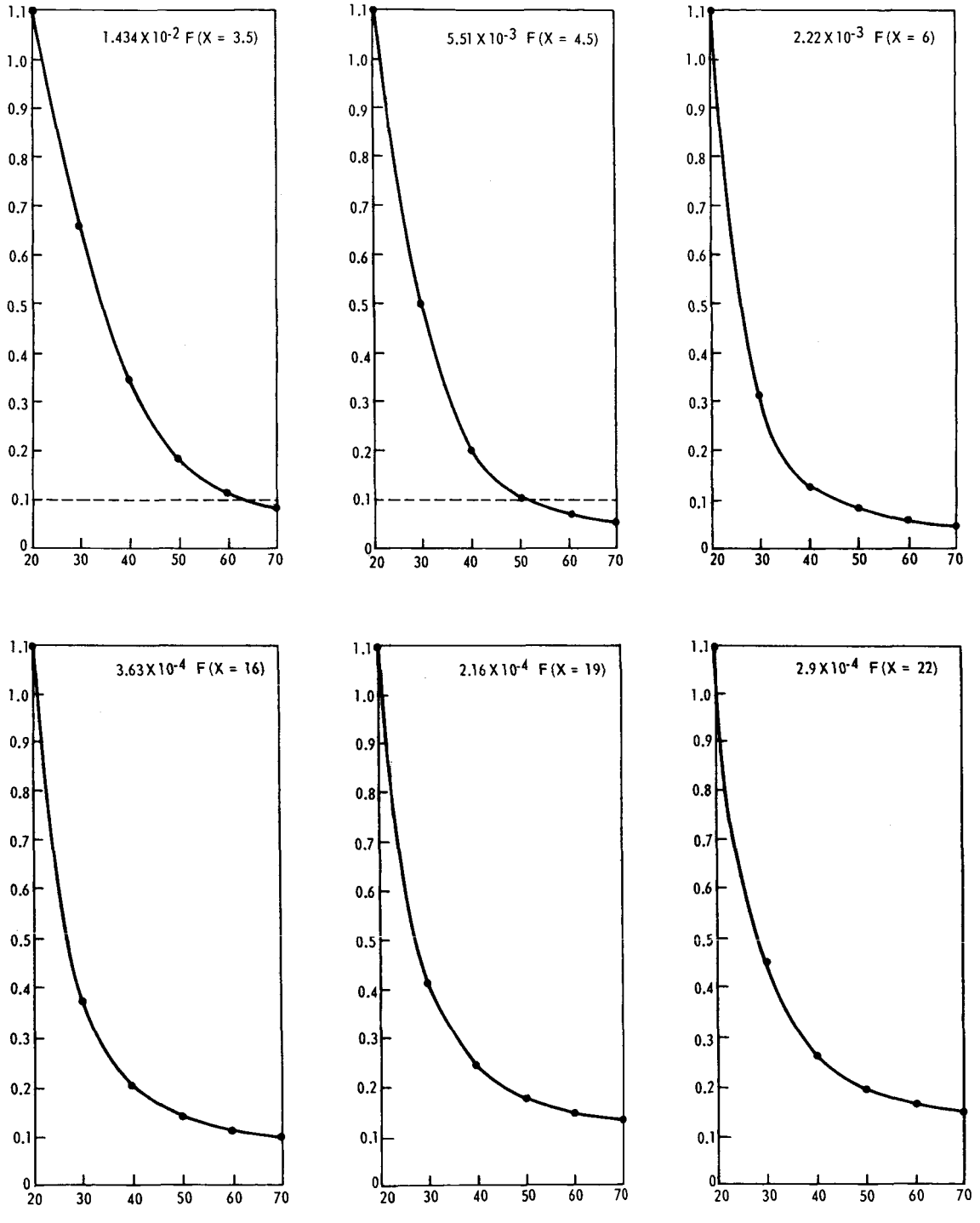

Figure 2C. (ϵ, m, X) Refractive Index m = 1.51 - 1.632 i

2

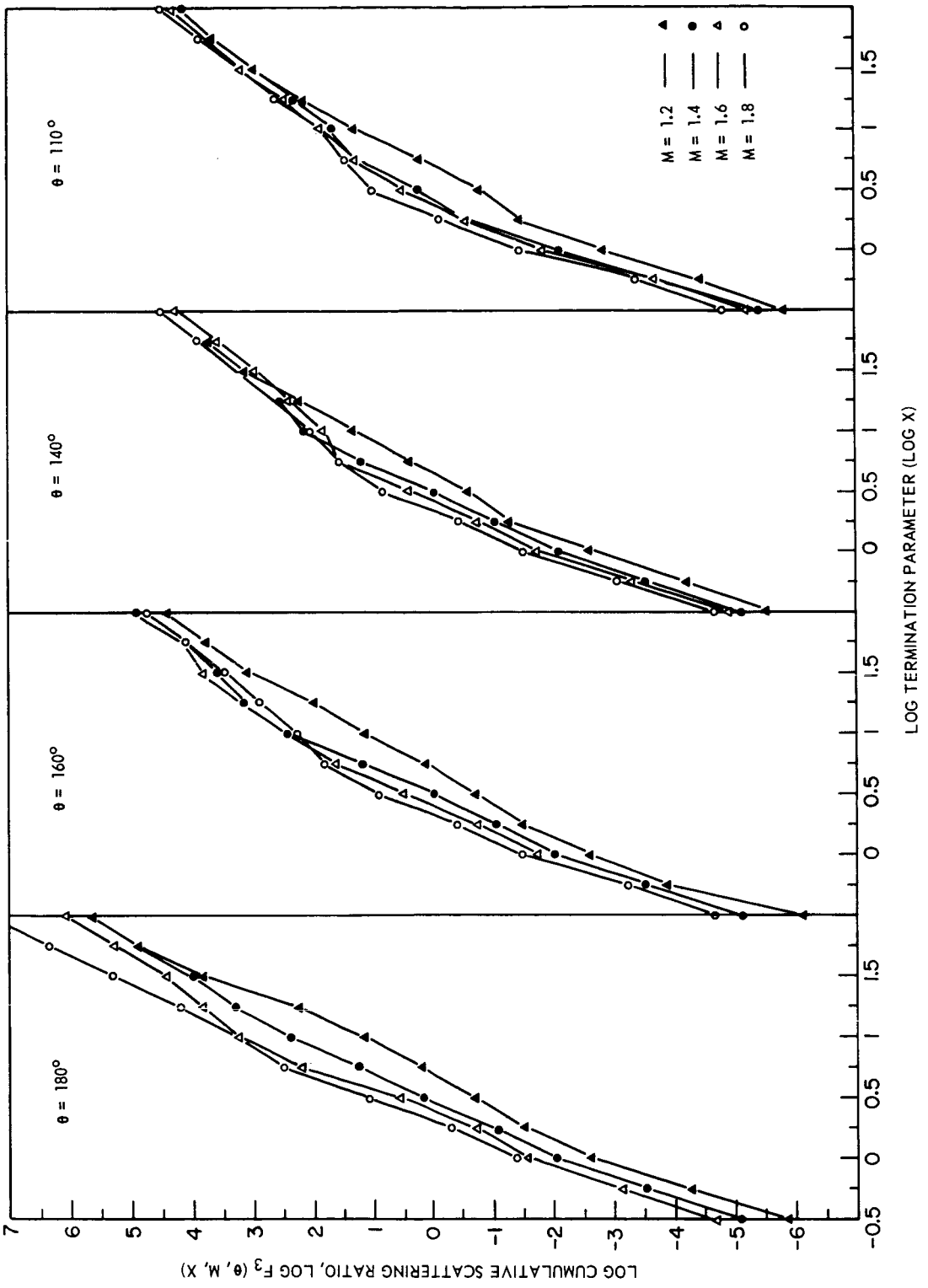

Figure 3A. Typical Mathematical Behavior of the Cumulative Brightness Function, F(X), for Various Values of the Scattering Angle, $\theta = \epsilon$, and Refractive Index, m. (taken from Powell and Donn, 1966)

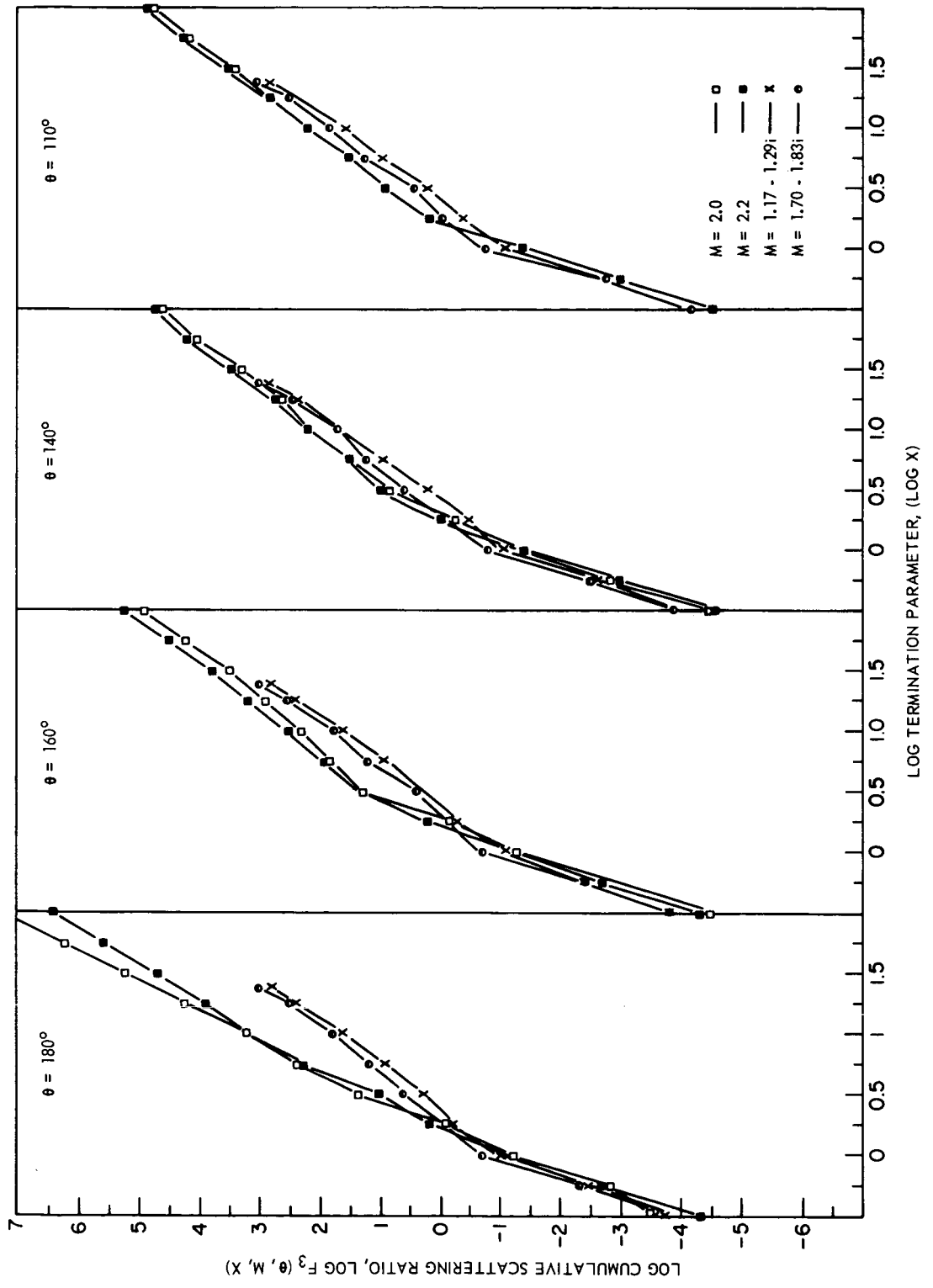

Figure 3B. Typical Mathematical Behavior of the Cumulative Brightness Function, F(X), for Various Values of the Scattering Angle, $\theta = \epsilon$, and Refractive Index, m. (taken from Powell and Donn, 1966)

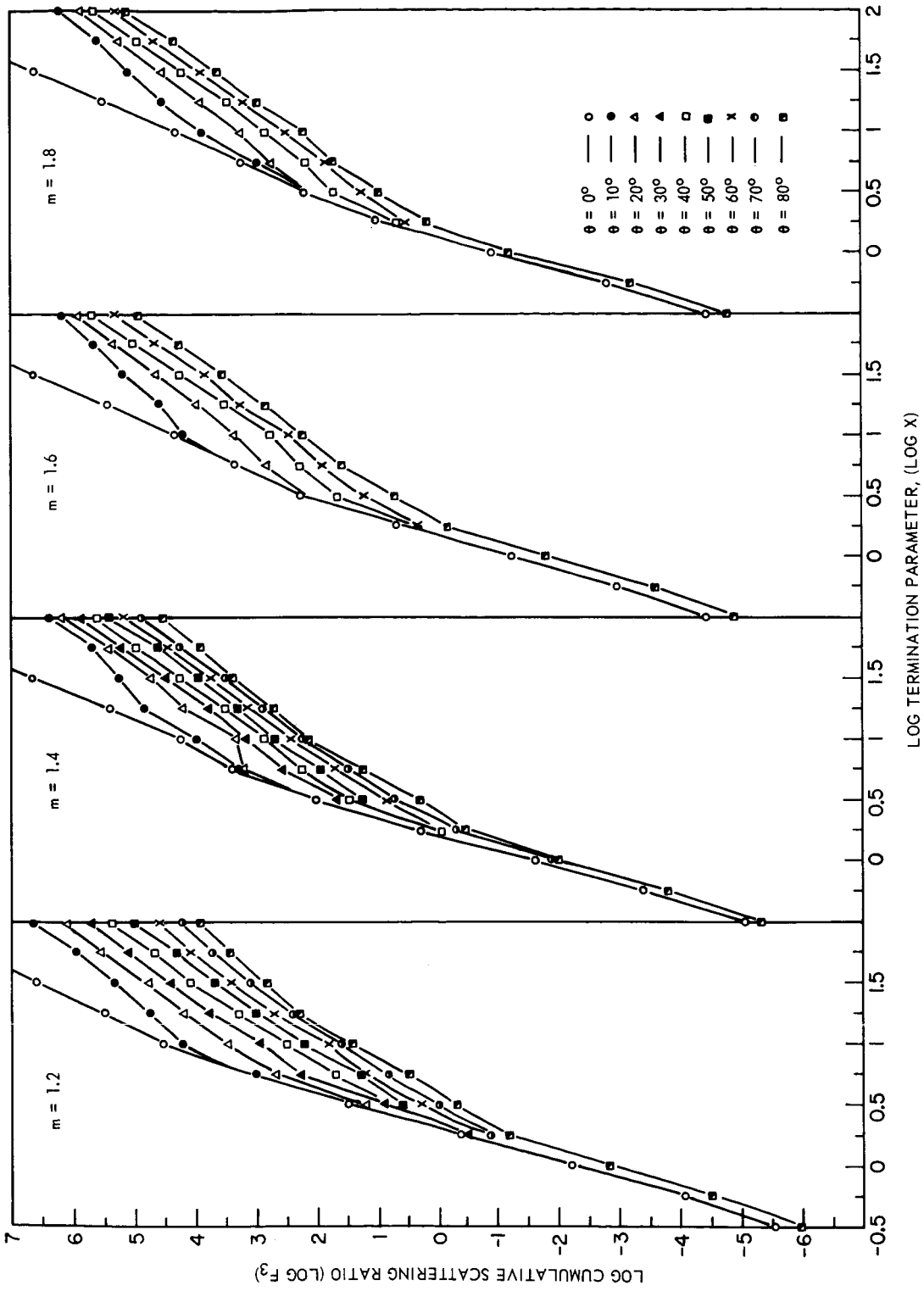

Figure 3C. Typical Mathematical Behavior of the Cumulative Brightness Function, F(X), for Various Values of the Scattering Angle, $\theta = \epsilon$, and Refractive Index, m. (taken from Powell and Donn, 1966)

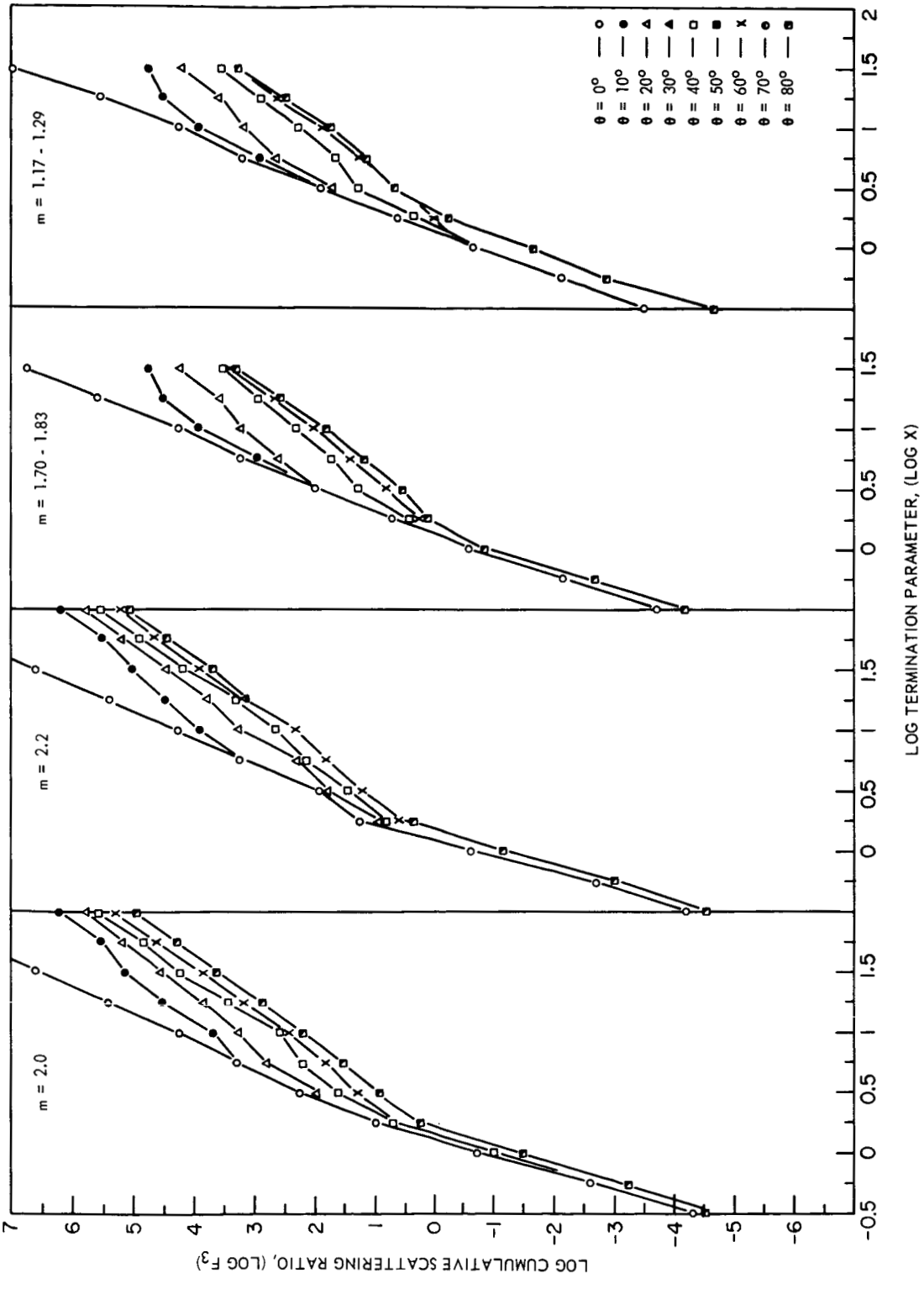

Figure 3D. Typical Mathematical Behavior of the Cumulative Brightness Function, F(X), for Various Values of the Scattering Angle, $\theta = \epsilon$, and Refractive Index, m. (taken from Powell and Donn, 1966)

An arbitrary, continuous size distribution of particles, $N(x)$, can always be expanded as a sum of terminated unit step functions with appropriate coefficients, $\overline{N}(X)$. i.e.:

$$N(x) = \sum_n \overline{N}(X_n)\ U(X_n) \tag{11}$$

Some of the coefficients, $\overline{N}(X_s)$, may be negative, indicating a lack of particles in the range defined by X_s. However, the sum of the negative coefficients, $\overline{N}(X_s)$, must be less than the sum of the positive coefficients, $\overline{N}(X_n > X_s)$, because a negative number of particles in any region has no physical meaning.

The scattering from the real size distribution of particles can now be simplified. First, notice that the measured brightness can be expanded as a sum of cumulative scattering functions:

$$\int_0^\infty N(x)\ i_j(\theta, m, x)\ dx \simeq \sum_n \overline{N}(X_n)\ F_j(\theta, m, X) \tag{12}$$

Substitute equation (12) into equation (8). Obtain:

$$B_j(\varepsilon, \lambda) = \frac{J_o R_o}{\sin^{1+\alpha}\varepsilon} \frac{\lambda^2}{8\pi^2} \sum_n \overline{N}(R_o, X_n) \int_\varepsilon^\pi \sin^\alpha\theta\ F_j(\theta, m, X_n)\, d\theta \tag{13}$$

Before simplifying equation (13) further in the next section, let us define the cumulative polarization function, $p(\theta, m, X_n)$. The polarization due to the unit step distribution function is:

$$p(\theta, m, X) = \frac{F_1(\theta, m, X) - F_2(\theta, m, X)}{F(\theta, m, X)} \tag{14}$$

as shown in figure 4. The measured polarization, P_m, due to all terminated step functions required to characterize an arbitrary continuous distribution, is given by:

$$P_m(\varepsilon, \lambda) = \frac{\sum_n \overline{N}(X_n, R_o) \int_\varepsilon^\pi \sin^\alpha\theta\ \Delta(\theta, m, X_n)\, d\theta}{\sum_n \overline{N}(X_n, R_o) \int_\varepsilon^\pi \sin^\alpha\theta\ F(\theta, m, X_n)\, d\theta} \tag{15}$$

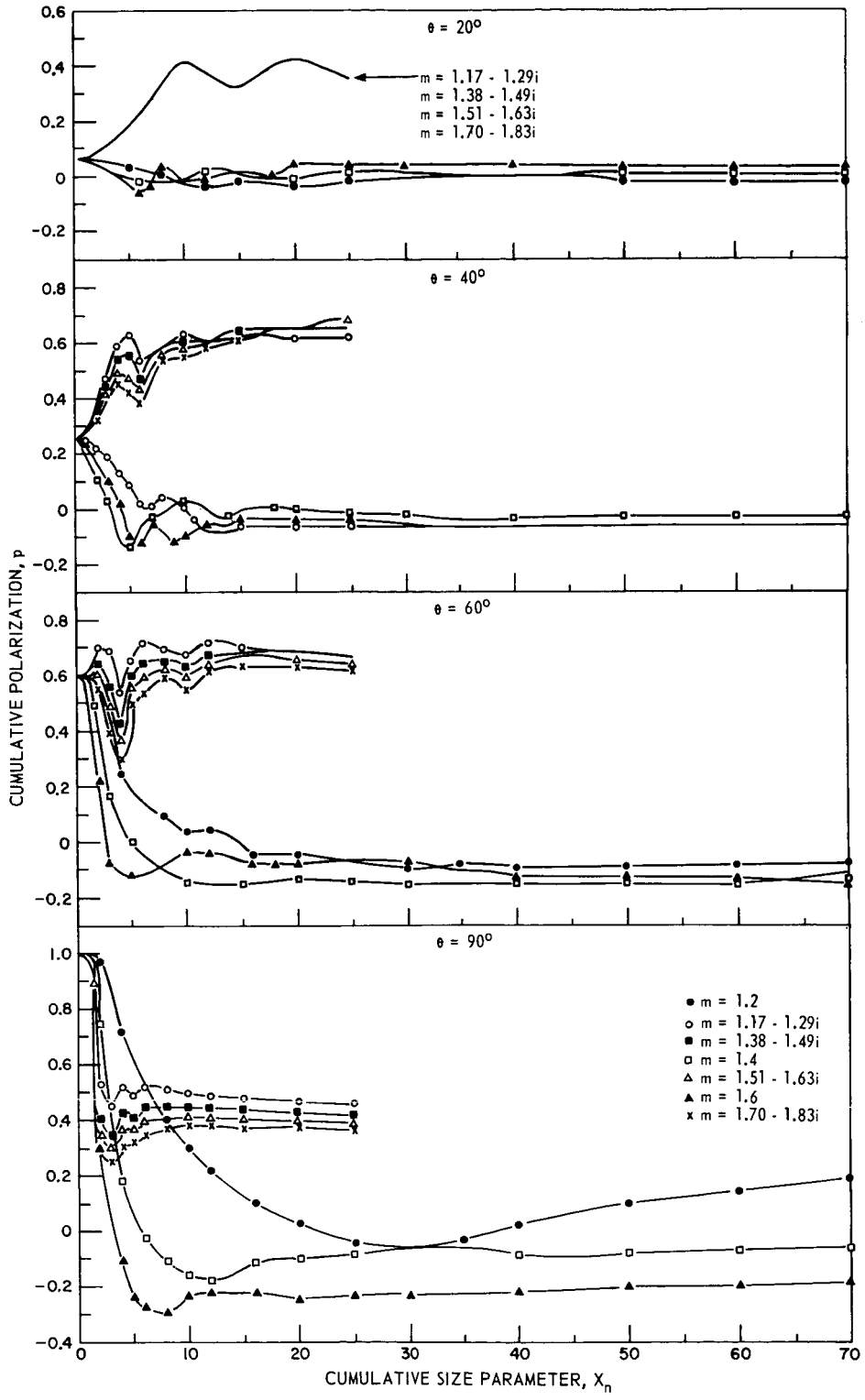

Figure 4A. Typical Behavior of the Cumulative Polarization Function, p(X) for Various Scattering Angles $\theta = \epsilon$ and Refractive Indices. (taken from Powell and Donn, 1966)

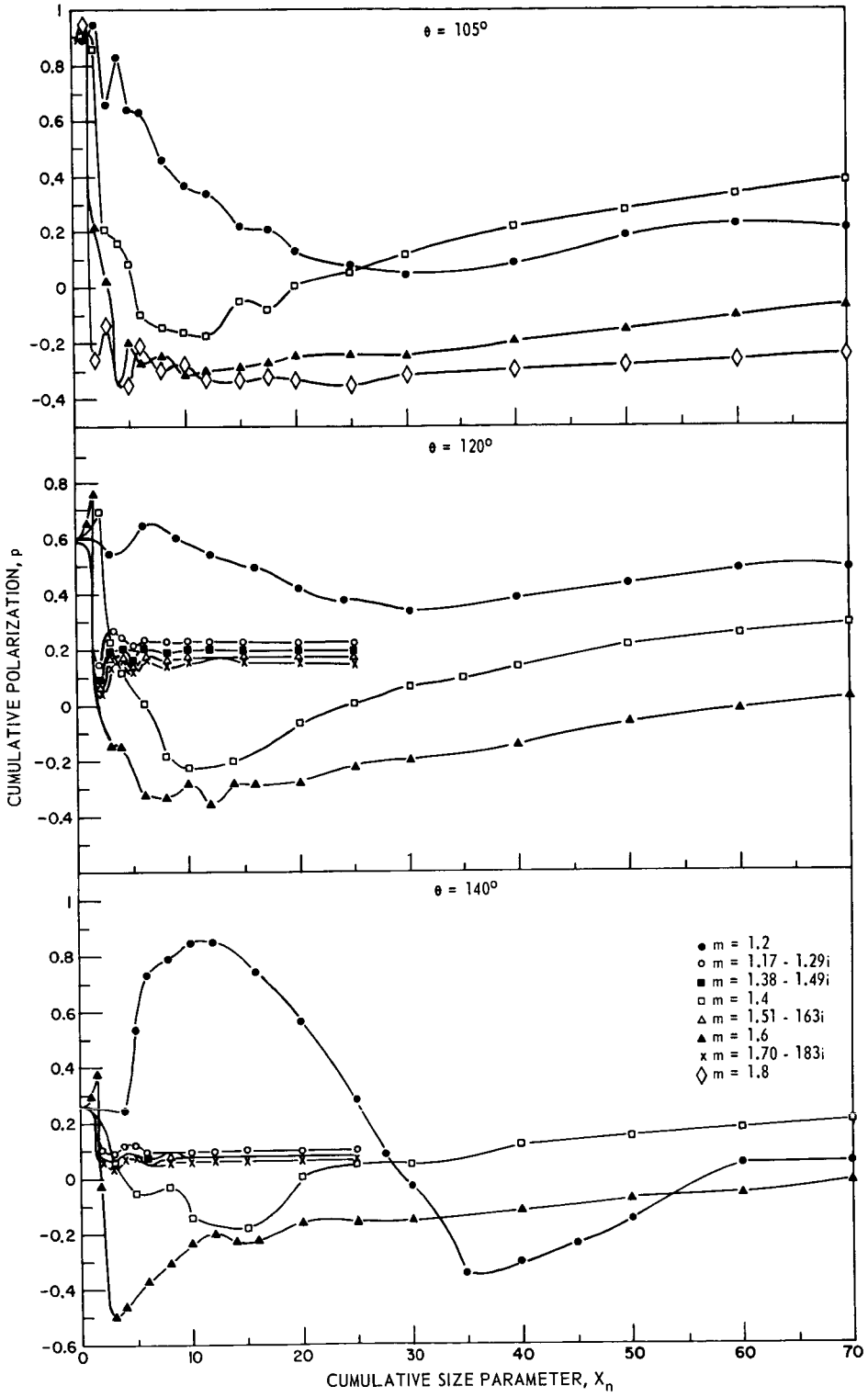

Figure 4B. Typical Behavior of the Cumulative Polarization Function, p(X) for Various Scattering Angles $\theta = \epsilon$ and Refractive Indices. (taken from Powell and Donn, 1966)

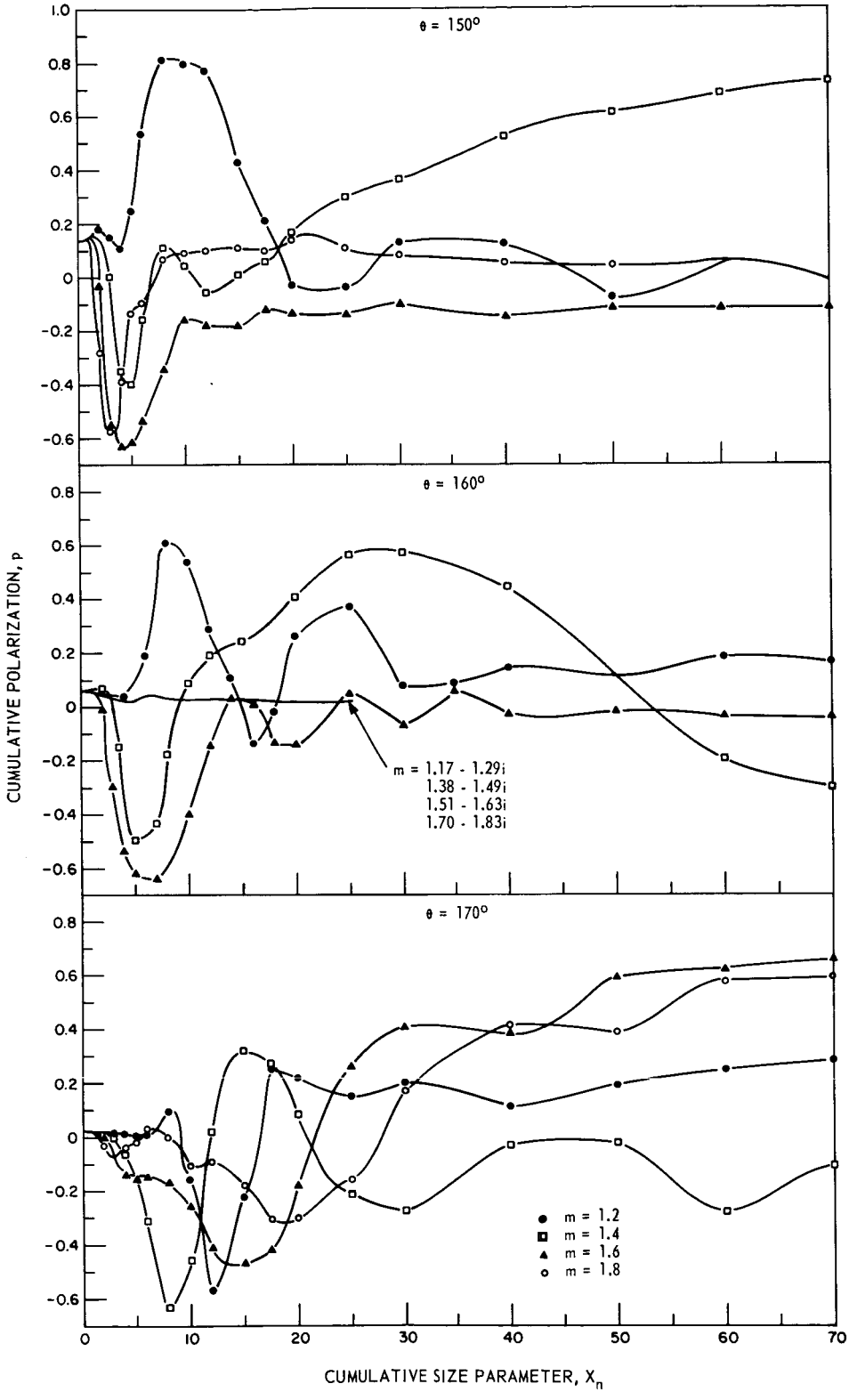

Figure 4C. Typical Behavior of the Cumulative Polarization Function, p(X) for Various Scattering Angles $\theta = \epsilon$ and Refractive Indices. (taken from Powell and Donn, 1966)

where:

$$\Delta(\theta, m, X_n) = F_1(\theta, m, X_n) - F_2(\theta, m, X_n)$$

$$= p(\theta, m, X_n)\, F(\theta, m, X_n) \qquad (16)$$

as shown in figure 5. The denominator of equation 15 is related to the measured brightness by equation (12). Thus:

$$B_m P_m \left(\frac{\sin^{1+\alpha}\varepsilon}{J_o R_o}\right) \frac{8\pi^2}{\lambda^2} = \sum_n \bar{N}(X_n, R_o) \int_\varepsilon^\pi \sin^\alpha\theta\, \Delta(\theta, m, X_n)\, d\theta \qquad (17)$$

2.3 Simplification of Equations (12) and (17)

Let us define two functions of the measured brightness and polarization:

$$M(\alpha, \varepsilon, \lambda) = B_m(\varepsilon, \lambda) \sin^{1+\alpha}\varepsilon \qquad (18)$$

and:

$$W(\alpha, \varepsilon, \lambda) = P_m(\varepsilon, \lambda)\, M(\alpha, \varepsilon, \lambda) \qquad (19)$$

From equations (12) and (17) we obtain:

$$M(\alpha, \varepsilon, \lambda) = K(\lambda) \sum_n \bar{N}(R_o, X_n) \int_\varepsilon^\pi \sin^\alpha\theta\, F(\theta, m, X_n)\, d\theta \qquad (20)$$

$$W(\alpha, \varepsilon, \lambda) = K(\lambda) \sum_n \bar{N}(R_o, X_n) \int_\varepsilon^\pi \sin^\alpha\theta\, \Delta(\theta, m, X_n)\, d\theta \qquad (21)$$

where:

$$K(\lambda) = J_o R_o \lambda^2/8\pi^2 \qquad (22)$$

Let:

$$\int_\varepsilon^\pi \sin^\alpha\theta\, F(\theta)\, d\theta = q(\pi) - q(\varepsilon) \qquad (23)$$

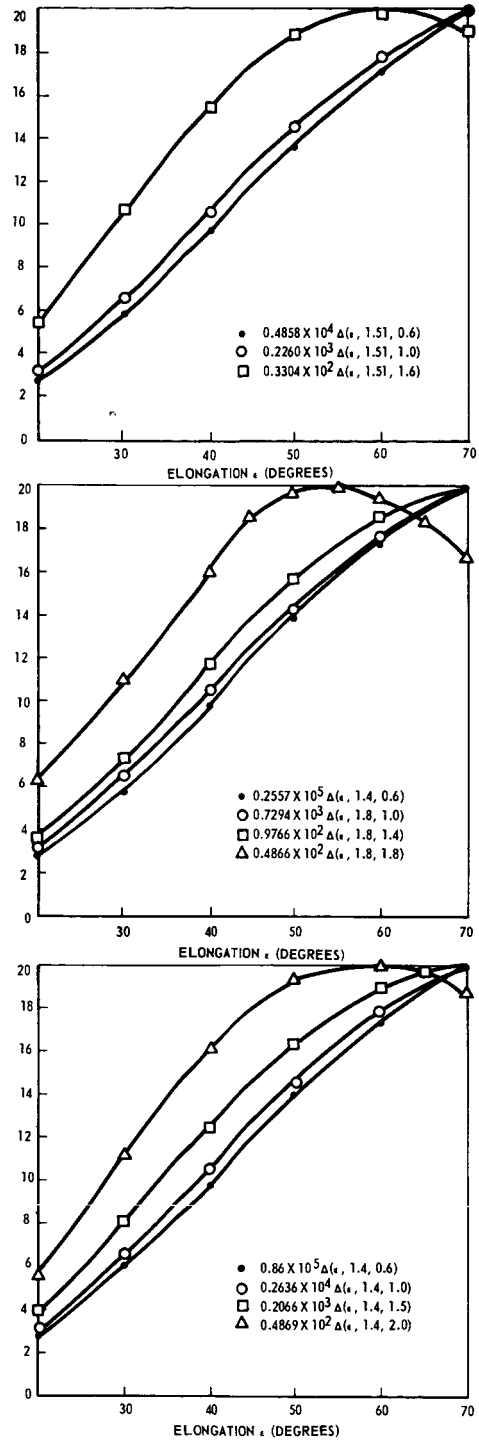

Figure 5A. Type 1 Functions, $\Delta(\epsilon, m, X)$, Characterized by Positive Value and Positive Slope

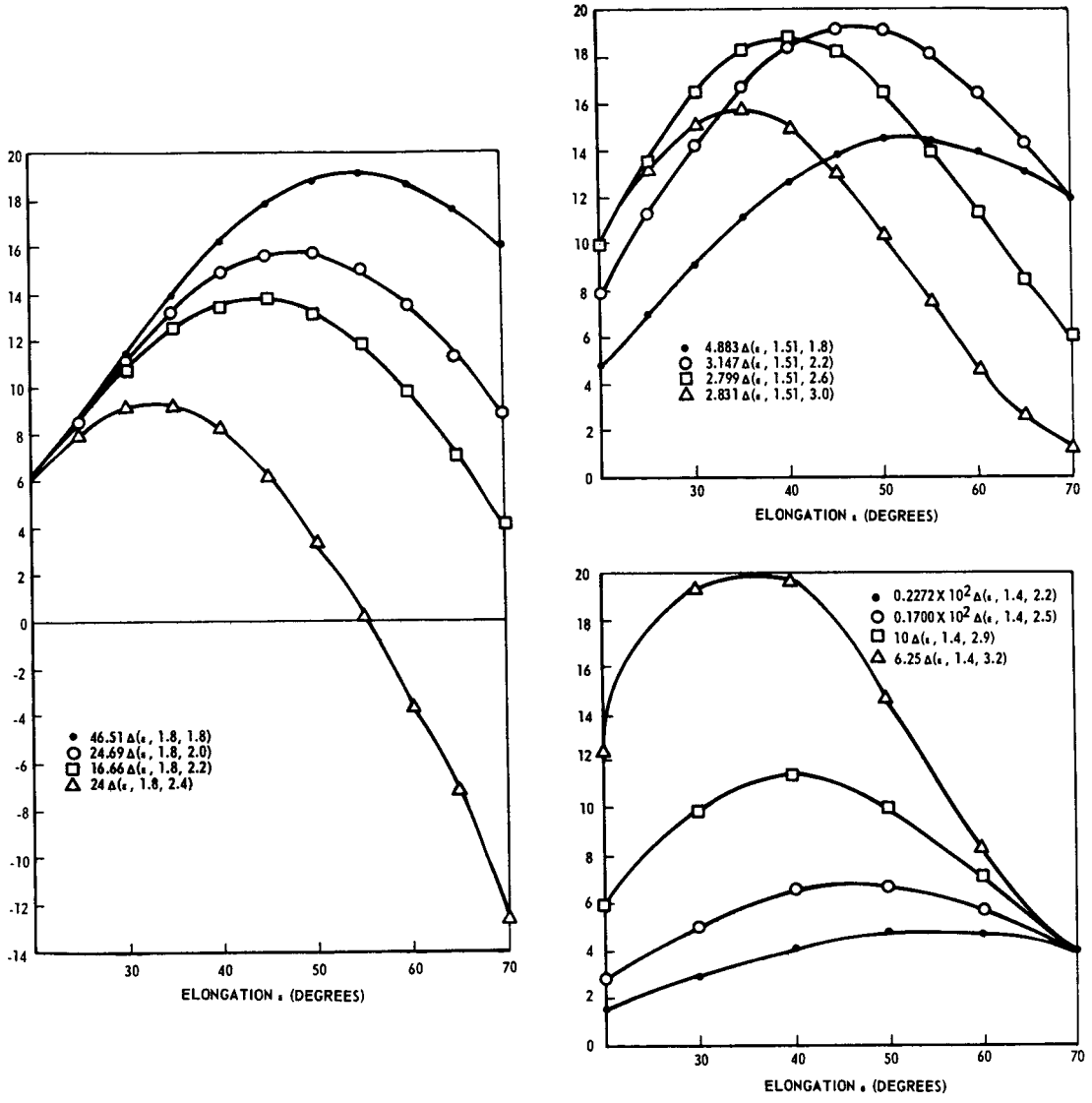

Figure 5B. Type 2 Functions, $\Delta(\epsilon, m, X)$, Characterized by Positive Value With Zero Slope Between 35° and 55°

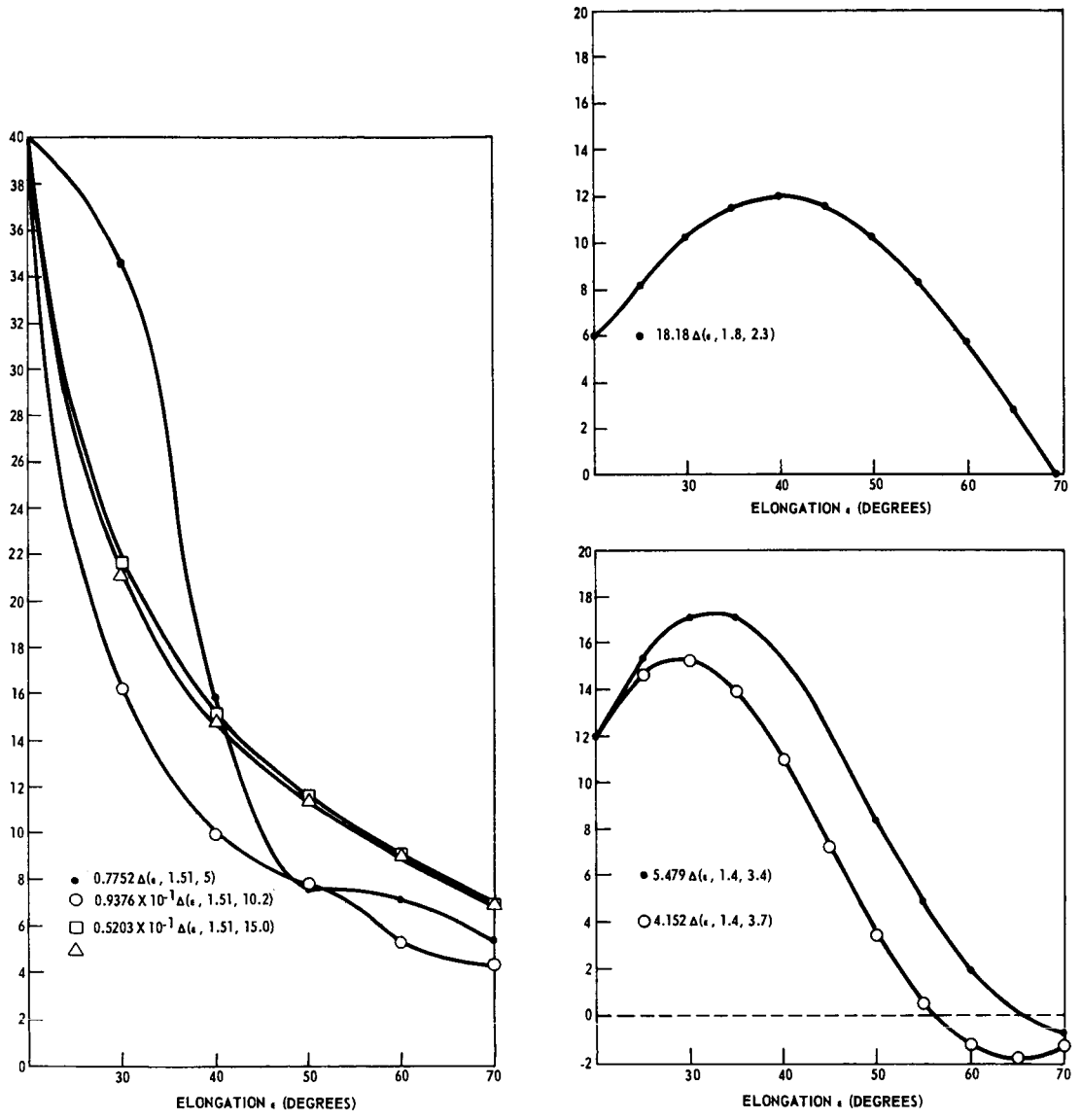

Figure 5C. Type 3 Functions, $\Delta(\epsilon, m, X)$, Characterized by Positive Value With a Negative Slope

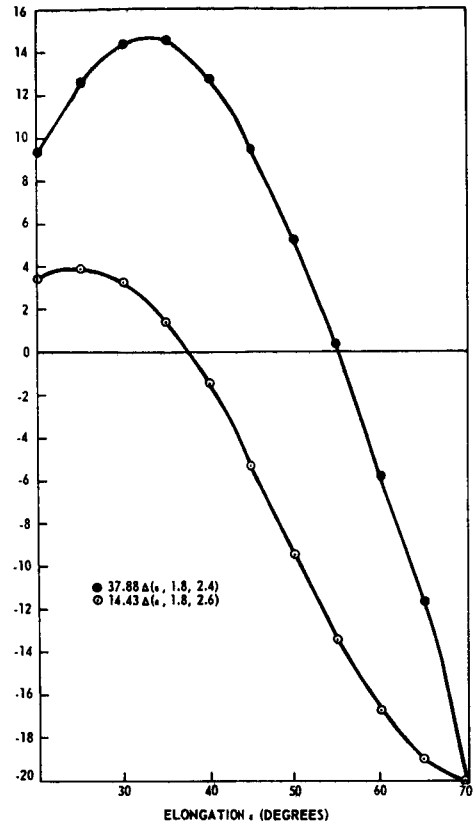

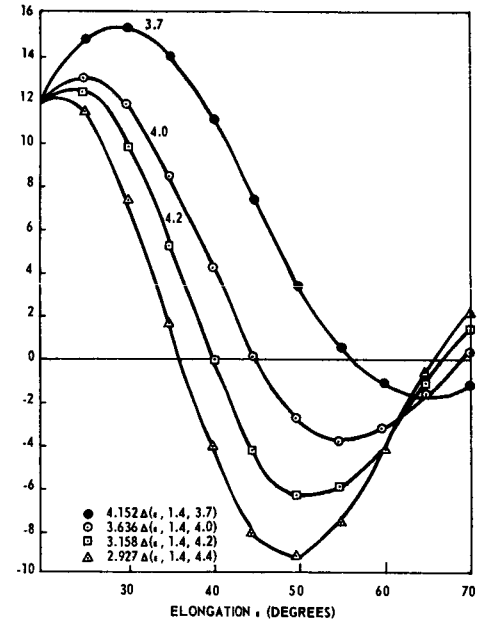

Figure 5D. Type 4 Functions, $\Delta(\epsilon, m, X)$, Characterized by Negative Slope and Both Positive and Negative Value

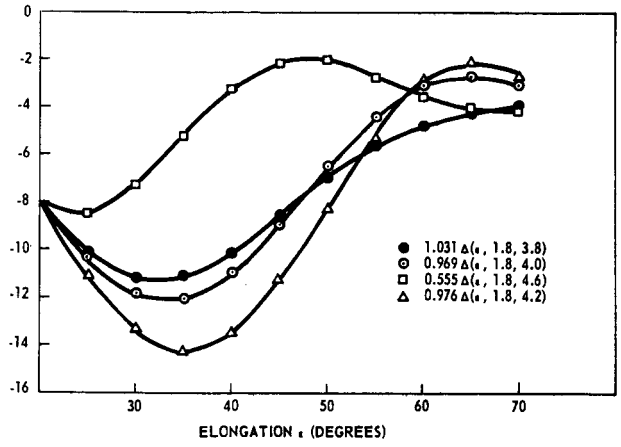

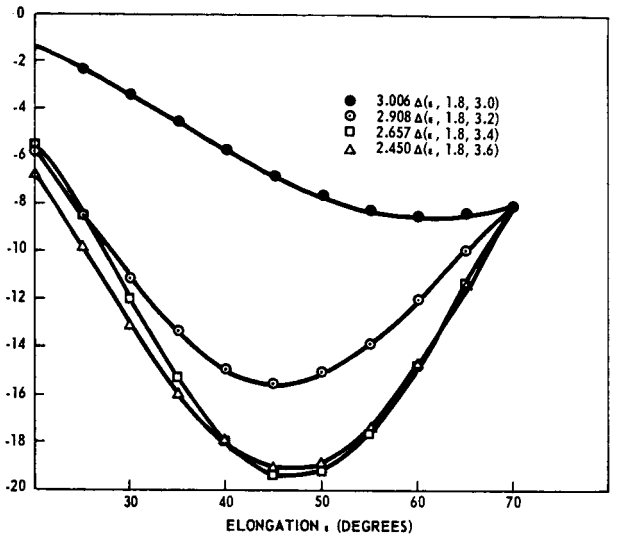

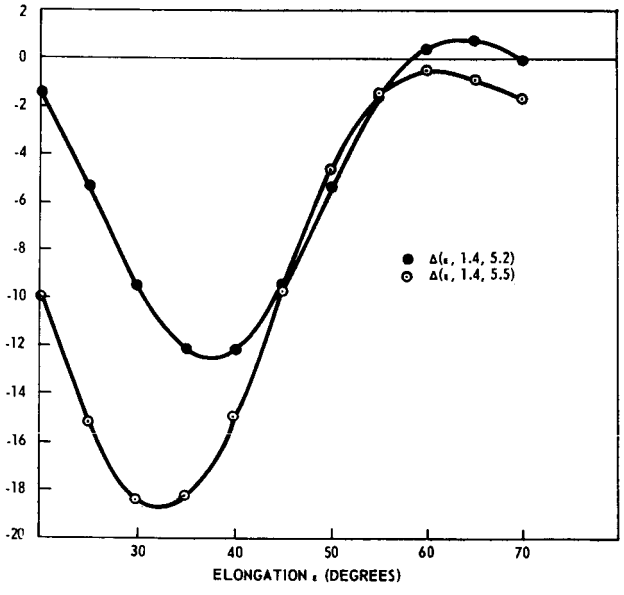

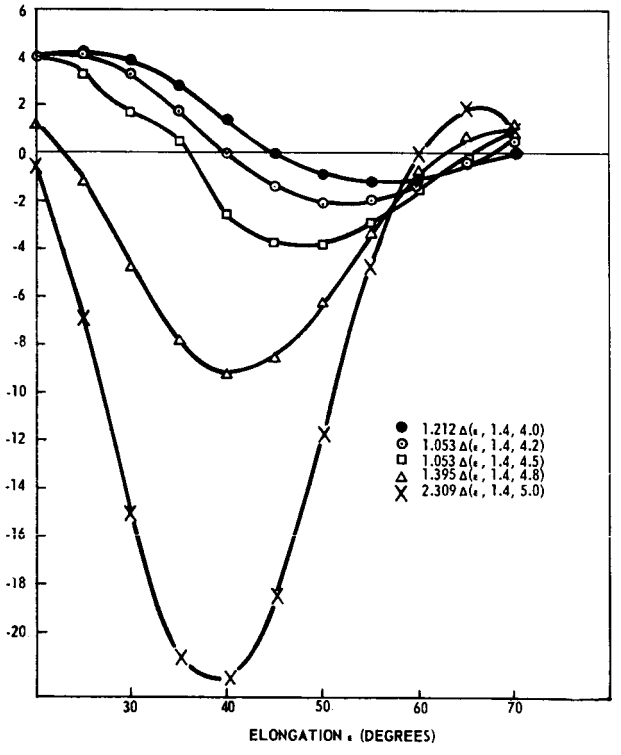

Figure 5E. Type 5 Functions, $\Delta(\epsilon, m, X)$, Characterized by Negative Values and Zero Slope Between 35° and 65°

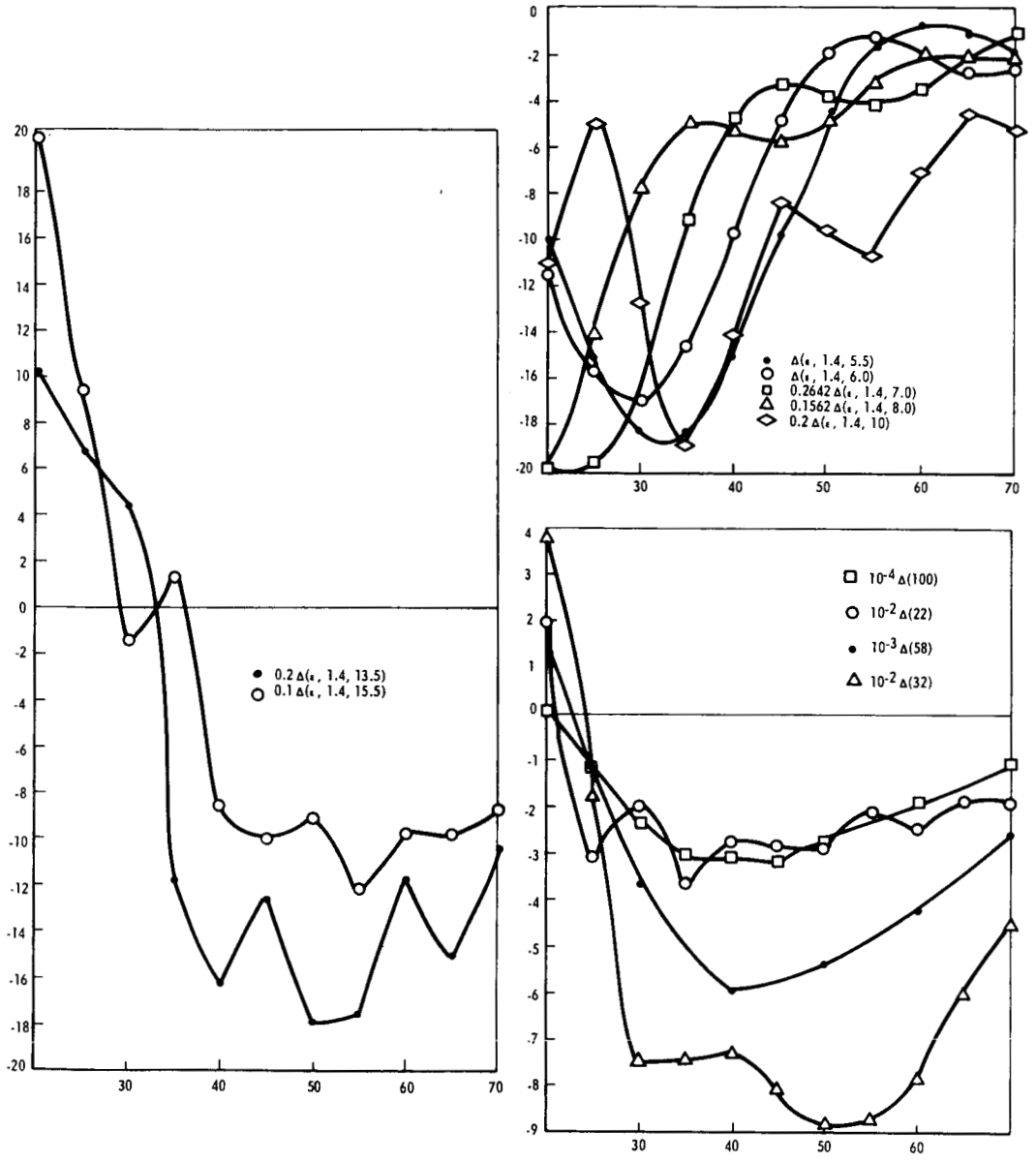

Figure 5F. Type 6 Functions, $\Delta(\epsilon, m, X)$, Characterized by Oscillatory Shape and Positive and Negative Values

and:

$$\int_{\varepsilon}^{\pi} \sin^{\alpha}\theta\ \Delta(\theta)\ d\theta = Q(\pi) - Q(\varepsilon) \tag{24}$$

Now, differentiate equations (20) and (21) with respect to ε, realizing that:

$$\frac{\partial q(\pi)}{\partial \varepsilon} = \frac{\partial Q(\pi)}{\partial \varepsilon} = 0$$

we obtain:

$$\frac{\partial M}{\partial \varepsilon} = -K(\lambda)\sum_{n} \overline{N}(R_o, X_n)\ \frac{\partial q}{\partial \varepsilon}$$

$$\frac{\partial W}{\partial \varepsilon} = -K(\lambda)\sum_{n} \overline{N}(R_o, X_n)\ \frac{\partial Q}{\partial \varepsilon}$$

but:

$$\frac{\partial q}{\partial \varepsilon} = \sin^{\alpha}\varepsilon\ F(\varepsilon)$$

$$\frac{\partial Q}{\partial \varepsilon} = \sin^{\alpha}\varepsilon\ \Delta(\varepsilon)$$

so:

$$\frac{\partial M}{\partial \varepsilon} = -K(\lambda)\sin^{\alpha}\varepsilon \sum_{n} \overline{N}(R_o, X_n)\ F(\varepsilon, m, X_n) \tag{25}$$

$$\frac{\partial W}{\partial \varepsilon} = -K(\lambda)\sin^{\alpha}\varepsilon \sum_{n} \overline{N}(R_o, X_n)\ \Delta(\varepsilon, m, X_n) \tag{26}$$

From equations (18) and (19) we also obtain:

$$\frac{\partial M}{\partial \varepsilon} = \frac{\partial B_m}{\partial \varepsilon}\sin^{1+\alpha}\varepsilon + (1+\alpha)\ B_m \sin^{\alpha}\varepsilon\cos\varepsilon \tag{27}$$

$$\frac{\partial W}{\partial \varepsilon} = \frac{\partial P_m}{\partial \varepsilon} B_m \sin^{1+\alpha}\varepsilon + P_m\left\{\frac{\partial B_m}{\partial \varepsilon}\sin^{1+\alpha}\varepsilon + (1+\alpha)\ B_m \sin^{\alpha}\varepsilon\cos\varepsilon\right\} \tag{28}$$

We define two new functions of the measured brightness and polarization:

$$S(\varepsilon, \lambda, \alpha) = \frac{-K^{-1}}{\sin^{\alpha}\varepsilon} \frac{\partial M}{\partial \varepsilon} \tag{29}$$

$$T(\varepsilon, \lambda, \alpha) = \frac{-K^{-1}}{\sin^{\alpha}\varepsilon} \frac{\partial W}{\partial \varepsilon} \tag{30}$$

Combining equations (25) through (30) we obtain:

$$S(\varepsilon, \bar{N}, X_n, m) = -\sum_n \bar{N}(R_o, X_n)\, F(\varepsilon, m, X_n) \tag{31}$$

$$T(\varepsilon, \bar{N}, X_n, m) = -\sum_n \bar{N}(R_o, X_n)\, \Delta(\varepsilon, m, X_n) \tag{32}$$

where S and T are obtained from the measured brightness, B_m, and polarization, P_m, for various assumed values of α and known λ as follows:

$$S_m(\varepsilon, \lambda, \alpha) = \frac{1}{K(\lambda)} \left\{ (1+\alpha) \cos\varepsilon\, B_m(\varepsilon, \lambda) + \frac{\partial B_m(\varepsilon, \lambda)}{\partial \varepsilon} \sin\varepsilon \right\} \tag{33}$$

$$T_m(\varepsilon, \lambda, \alpha) = \frac{1}{K(\lambda)} \left\{ B_m \left[\sin\varepsilon \frac{\partial P_m}{\partial \varepsilon} + (1+\alpha) P_m \cos\varepsilon \right] + P_m \frac{\partial B_m}{\partial \varepsilon} \sin\varepsilon \right\} \tag{34}$$

Equations (31) through (34) represent the fundamental mathematical relationships between optically measureable quantities and the physical properties of the interplanetary dust. The measured functions $S_m(\varepsilon)$ and $T_m(\varepsilon)$ can be obtained directly from the observed curves and plotted for various assumed values of α. The resulting curves are smooth and continuous for $\varepsilon > 20^{\circ}$ as shown, for example, in figures 6 and 7 taken from the observations of Blackwell and Ingham.

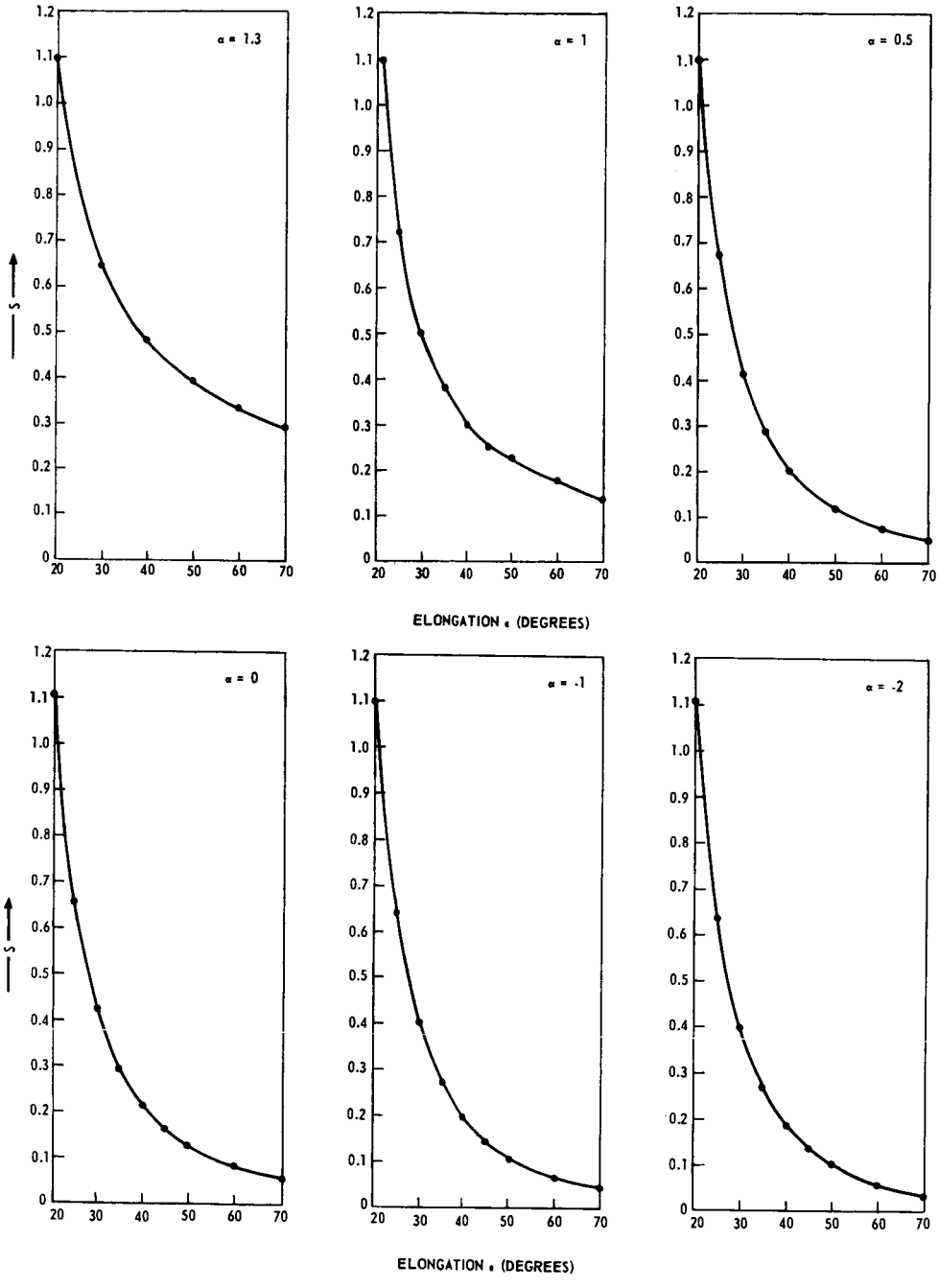

Figure 6. The Function $S_m(\epsilon, \alpha)$ Calculated From the Observations of Blackwell and Ingham is Shown for Various Assumed Values of α. $S_m(\epsilon, \alpha)$ is Defined by Equation 33.

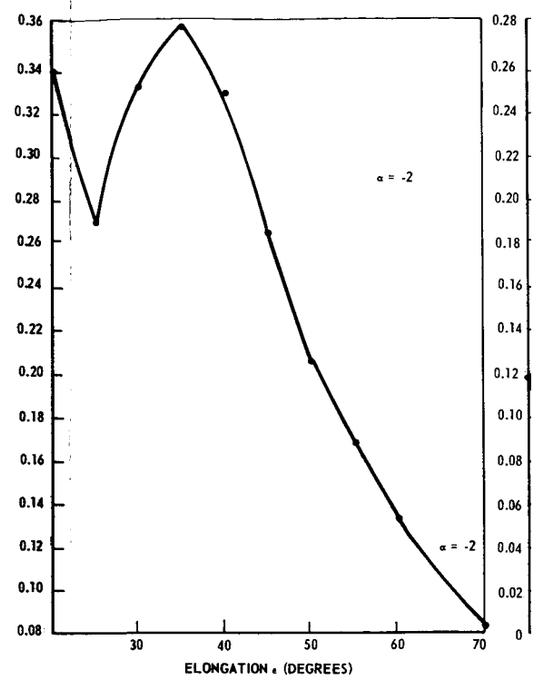

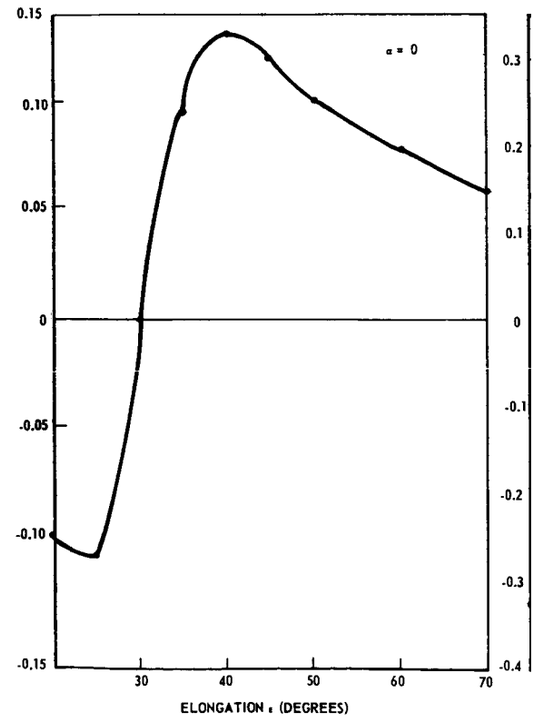

Figure 7.

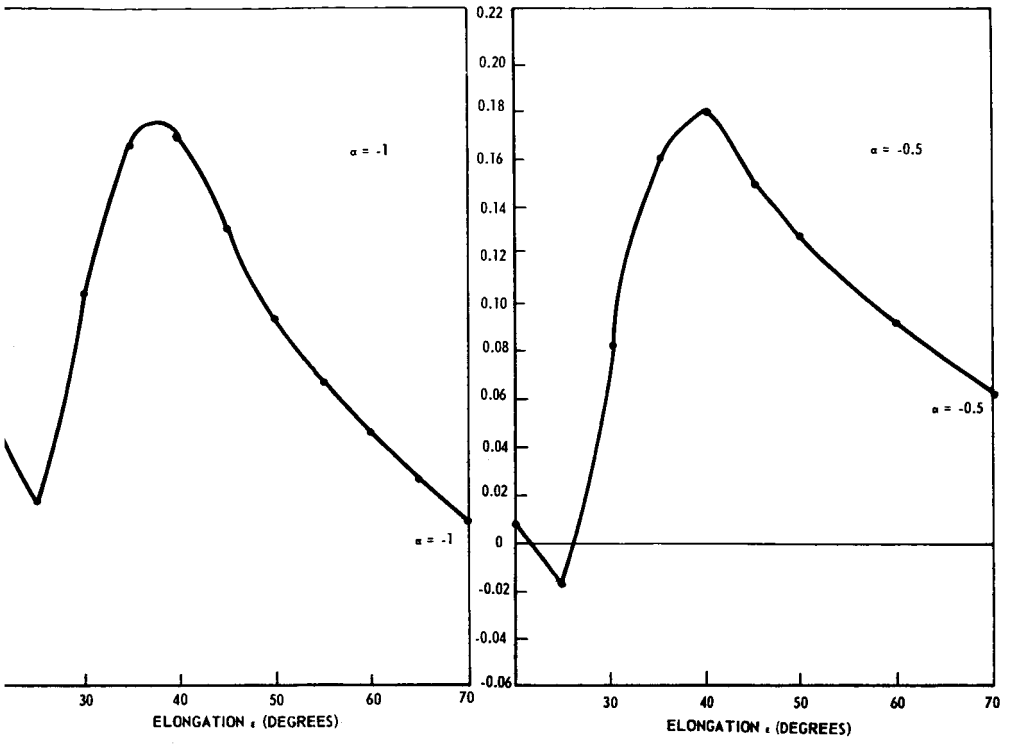

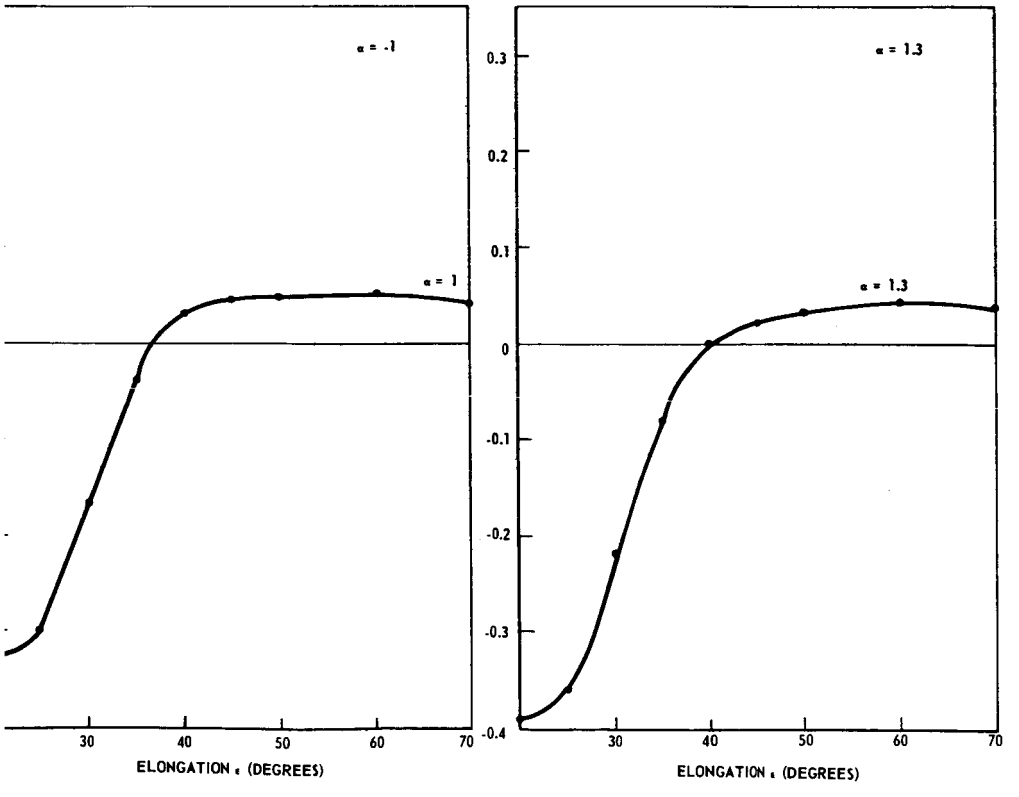

The Function $T_m(\epsilon, \alpha)$ Calculated from the Observations of Blackwell and Ingham is Shown for Various Assumed Values of α, $T_m(\epsilon)$ is Defined by Equation 34.

2

3. ANALYTIC METHOD

The "measured" curves $S_m(\epsilon)$ and $T_m(\epsilon)$ obtained by combining B_m, $\partial B_m/\partial\epsilon$, P_m and $\partial P_m/\partial\epsilon$ according to equations 33 and 34, must be matched by a sum of theoretical curves, $F(\epsilon,m,X_n)$ and $\Delta(\epsilon,m,X_n)$, as in equations 31 and 32 with appropriate coefficients, $\overline{N}(R_o,X_n)$, in order to determine the unknowns m,X_n and $\overline{N}(R_o,X_n)$. This is accomplished as follows:

First, note the unique characteristics of the measured curves S_m and T_m. They can be characterized by their magnitude, sign, slope and the elongations at which peaks and valleys occur for various assumed values of α.

Second, investigate the behavior of the curves $F(\epsilon)$ or $\Delta(\epsilon)$ for various values of m and X_n. $F(\epsilon)$ may be characterized by its slope in two regions, $0<\epsilon<70°$ and $110°<\epsilon<180°$, and the elongation angle at which $F(\epsilon)$ is a minimum, $70°<\epsilon<110°$. For example, $F(\epsilon)$ for $0<\epsilon<70°$ is presented graphically for various representative values of X_n and m in figure 2. The function $\Delta(\epsilon,m,X_n)$ is grouped into six different classification depending on whether the function is in general positive or negative, and/or whether it exhibits positive or negative slope. $\Delta(\epsilon)$ is shown graphically for representative values of m and X_n in figures 5A - 5F for $0<\epsilon<70°$. The A series corresponds to group 1 types, the B series to group 2 types, etc. In general as we go from group one to group six, X_n increases for all values of m. Almost any combination of positive and negative values with a positive or negative slope is available. $\Delta(\epsilon)$ may be either positive or negative when the refractive index, m, is real (non-absorbing particles). On the other hand if m has an imaginary component (absorbing particles), $\Delta(\epsilon)$ is positive for all values of X_n and ϵ.*

Third, choose various values of m and X_n for which the corresponding curves $F(\epsilon)$ and $\Delta(\epsilon)$ show characteristics similar to the measured curves $S_m(\epsilon)$ and $T_m(\epsilon)$. For example, if the curve $S_m(\epsilon)$ shows a steep negative slope, choose a curve $F(\epsilon)$ for $X_n > 5$; if $T_m(\epsilon)$ is negative over a given range in ϵ, choose m real and X_n such that $\Delta(\epsilon)$ is also negative in that range. Choose as many different $F(\epsilon,m,X_n)$ or $\Delta(\epsilon,m,X_n)$ as there are measured points in the curves S_m or T_m. Choose at least one X in each of the six $\Delta(\epsilon)$ catagories.

Fourth, substitute the chosen function $F(\epsilon)$ and $\Delta(\epsilon)$ into equations 31 and 32 thereby obtaining as many equations as there are measured points on the curves $S_m(\epsilon,\alpha)$ and $T_m(\epsilon,\alpha)$. The resulting matrix equations can be programed directly from the graphs in figures 2 and 5.

---

* A preliminary investigation by Donn and Powell (unpublished) indicates that $\Delta(\epsilon,X_n)$ is positive for all ϵ and X_n even when the absorption coefficient is only 1/4 of the real part.

Fifth, solve the matrix equations for $\bar{N}(R_o,X_n)$. Negative values of $\bar{N}(R_o, X_n)$ will probably appear in the first solution. These are only permissible if the magnitude of the negative coefficient, say $\bar{N}(R_o,X_s)$, is less than the sum of the positive coefficients, $\bar{N}(R_o,X_{p>}X_s)$.

Sixth, find a set of curves, $\Delta(\epsilon,m,X_n)$, which, when summed with proper coefficients, match the product, $\bar{N}(\epsilon,X_s)\Delta(\epsilon,X_s)$, corresponding to nonpermissible negative coefficients $\bar{N}(\epsilon,X_s)$. Most functions $\Delta(\epsilon,m,X_n)$ can be expanded in terms of a sum of other Δ functions with different termination parameters, X, or different refractive indices, m. A four-term expansion is usually sufficient, so that the computer is not required for this step.

3.1 Limiting Values of α.

The cumulative scattering ratios, $F(\epsilon,m,X)$, all have negative slopes in the region $\theta<\epsilon< 90^o$. Also, they are positive for all values of ϵ, m and X. This fact, when correlated with slope of the measured function, S_m, immediately places an upper limit on the value for α. As can be seen from equation 5, a given value for α corresponds to a given increase ($\alpha<0$) or decrease ($\alpha>0$) in the particle number density as the particle orbital radius increases. According to equations 31 and 33:

$$-K\sum_n \bar{N}(R_o,X_n)F(\epsilon,m,X)=B_m\left\{(\alpha+1)\cos\epsilon - b\,\frac{\sin\epsilon}{\epsilon}\right\} \qquad (35)$$

where b is the log-log slope of the measured brightness curve, $B_m(\epsilon)$, in the range $20^o<\epsilon< 70^o$. i.e.

$$B_m \simeq B_o \epsilon^{-b}$$

The summation on the left side of equation (35) is always positive, so:

$$b\,\frac{\sin\epsilon}{\epsilon} \geq (\alpha+1)\cos\epsilon \qquad (36)$$

for $20^o<\epsilon<70^o$.

Finally:

$$\alpha<b-1 \qquad (37)$$

From Blackwell and Ingham's data, $b\simeq 2.48$. Equation 37 becomes:

$$\alpha<1.48$$

Weinberg's measured brightness gives nearly the same result. The values of α estimated by Giese and Siedentopf (1962) for dielectric particles are clearly too high. Their derived mixtures contain dielectric particles with $\alpha=3$ and $\alpha=3.5$.

4. UNIQUENESS

The brightness and polarization of the light scattered by an ensemble containing monodisperse, spherical particles can only be expressed as a slowly converging series. Each term is a complicated function of the particle size parameter, refractive index and scattering angle. Physically, the n^{th} term represents the radiative effect of a $2n^{th}$ order electric or magnetic multipole stimulated in the particle by the incident fields. The interference between radiation from multipoles of different order produces resonance for some combinations of the variables x, θ, m, and dissonance for others. Consequently the apparent brightness and polarization is an erratically oscillating function of these variables. When the particles are monodisperse their size and refractive index can be determined uniquely by analyzing the spectral and angular position of the various peaks and valleys in the measured brightness and polarization curves.

There are three reasons for suspecting the uniqueness of deductions based on observations of the zodiacal light. Each has to do with effects that blur the resonances and dissonances which are so characteristic of monodisperse particles. In addition, there is no reliable information concerning the spectral character of the zodiacal light. Thus, all deductions concerning the nature of the particles must be based on the angular variations in the scattered light at one wavelength. As it turns out, the angular measurements are more uniquely representative of the particle ensemble than we initially suspected.

4.1 Geometrical Ambiguities

We were most concerned with ambiguities resulting from the observational geometry of the zodiacal light. The field of view accepts light from all scattering angles, $\theta > \epsilon$. From equation 8, one might therefore expect that characteristic angular resonances and dissonances would be averaged out by the integration over θ even if the particles were monodisperse. By following the logic leading to equations (31) through (34), it can be seen that the angular integration is unnecessary. The integral is removed by proper combination of the measured functions B_m, P_m, $dB_m/d\epsilon$ and $dP_m/d\epsilon$. Consequently, the measured functions $S_m(\epsilon)$ and $T_m(\epsilon)$ are as uniquely descriptive of monodisperse particles as are the Mie functions $i_j(\epsilon, m, x)$. The observational geometry of the zodiacal light does not affect the uniqueness of deductions concerning the nature of the particles.

4.2 Ambiguities Due to Polydispersion

The second reason for suspecting the uniqueness of deductions from zodiacal light observations is due to the fact that the interplanetary dust

ensemble probably contains particles of all sizes. The resulting integral:

$$\int_0^\infty N(x) i_j(x) dx$$

therefore averages out the distinctive resonances in the Mie functions $i_j(x)$. (A typical Mie function is shown in figure 8, for example.)

Assume that the refractive index of the particles is known. As stated in paragraph 2.2 (equation 11), any size distribution function, $N(x)$, may be expanded as a sum of terminated unit step functions, $U(X)$, with coefficients, $\overline{N}(X)$. To each unit step, containing particles with size parameters $0<x<X$ there corresponds two cumulative functions, F and Δ, which describe the integrated optical character of the particles (equations 10 and 16). The uniqueness with which $\overline{N}(X_n)$ and X_n may be deduced from equations 31 and 32 therefore depends upon proving the validity of the following propositions:

Proposition I : The pair of curves $F(\epsilon, X_i)$ and $\Delta(\epsilon, X_i)$ are sensitive and unique functions of X_i for known refractive index m.

Proposition II : The pair of curves $F(\epsilon, X_i)$ and $\Delta(\epsilon, X_i)$ cannot be expressed as linear combinations of other pairs $F(\epsilon, X_k)$ and $\Delta(\epsilon, X_k)$ for $k \neq i$, i.e. either on both of the following inequalities are valid for all ϵ:

$$F(\epsilon, X_i) \neq \sum A_k F(\epsilon, X_k) \qquad (38)$$

$$\Delta(\epsilon, X_i) \neq \sum A_k \Delta(\epsilon, X_k) \qquad (39)$$

Neither of the above propositions can be proved valid for all X. By studying the curves in figures 2 and 5 it can be appreciated that Proposition I is valid for $X < 20$*. $\Delta(\epsilon)$ is a very sensitive function of X. Since

---

* Ambiguities in determining $\overline{N}(X)$ and X for $X > 20$ are probably not serious. The size distribution of the interplanetary dust probably exhibits a sharp peak at $x < 20$ and a long tail for $x > 20$. The lower order moments are independent of the number of large particles ($x > 20$) and the higher order moments are independent of the frequency interval for $x > 20$. The histographic approximation, $N(x) = \sum \overline{N}(X_n)\, U(x_n)$, is therefore roughly independent of which X_n is chosen in the interval $X > 30$.

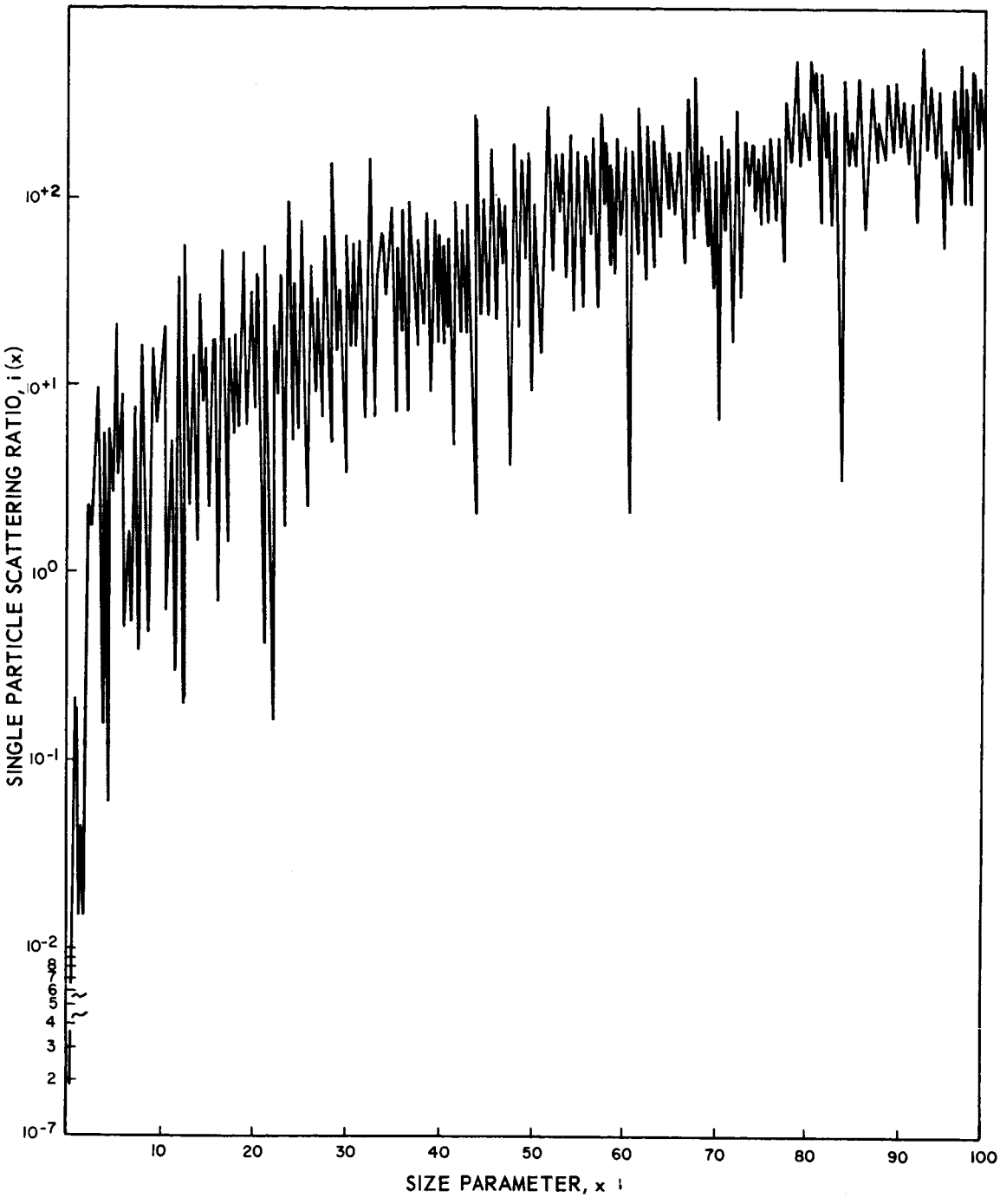

Figure 8. Typical Resonance Behavior of the Mie Function $i_j(X)$

its mathematical behavior is so different in each of the six categories defined in figure 5, proposition I is obviously valid for at least six X_i in the range $0<X_i<100$ as shown, for example, in table I.

TABLE I

GROSS MATHEMATICAL CHARACTER OF $\Delta(\epsilon)$ for $20^\circ<\epsilon<70^\circ$

Category	X	$\Delta(\epsilon)$	$d\Delta/d\epsilon$	
1	$0<X<1.8$	+	+	
2	$1.8<X<2.2$	+	0	$(35^\circ<\epsilon<55^\circ)$
3	$2.2<X<2.6$	+	-	
4	$2.6<X<3.0$	+ or -	-	
5	$3.0<X<3.6$	-	0	$(35^\circ<\epsilon<65^\circ)$
6	$X>4$	+ and -	+ and -	

As can be gleaned from figure 4 showing $p(\epsilon)$, $\Delta(\epsilon)$ may be further classified when measurements are available in the range $70^\circ<\epsilon<180^\circ$. There are at least 30 grossly different and unique $\Delta(\epsilon, X_n)$ in the range $0<X_n<100$.

We have attempted to disprove proposition II by trying to find simultaneous linear expansions to contradict equations 38 and 39. It is possible to find such expansions in contradiction to either equation 38 or 39. However, $F(\epsilon, X_n)$ is a completely different sort of mathematical function than $\Delta(\epsilon, X_n)$. Thus, it is improbable the coefficients, A_k, determined by linear expansion in contradiction to equation (39) will be solutions to contradict equation (38) for the same values of X_k.

In summary: We are confident that solutions to equations 29 and 30 are unique when the refractive index is known, but we cannot justify our confidence by an unqualified mathematical proof.

4.3 Ambiguities Due to Heterogeneity

The third reason for suspecting the uniqueness of deductions for zodiacal light observations is due to the fact that the interplanetary dust ensemble probably contains a mixture of particles with different refractive indices. Two questions occur: (1) how do deductions regarding the size distribution of the interplanetary dust depend upon the refractive index of the particles, and, (2) can one deduce the refractive indices in the mixture from zodiacal light observations?

As can be seen from figure 3 the function $F(\epsilon,m,X)$ is not a sensitive function of refractive index even when observations are made at several wavelengths. Thus, equations 31 and 33 can be matched for a given size distribution independently of the composition of the particles.

$\Delta(\epsilon,m)$ is more sensitive to changes in m for a given X but, as can be seen from figure 5, the mathematical behavior of each category in the range $20^{\circ}<\epsilon<70^{\circ}$ is roughly independent of the refractive index. Particles with a given refractive index tend to polarize like larger particles with a smaller refractive index but the effect is not large enough to cause appreciable changes in the deduced size distribution.

Study of the cumulative polarization function, $p(m)$, shown in figure 4, is most appropriate in order to understand the optical effects due to refractive index. Equation 32 may be rewritten:

$$T_m(\epsilon,\lambda,\alpha) = -\sum \bar{N}(R_o,X_n) \quad F(\epsilon,m,X_n) \quad p(\epsilon,m,X_n)$$

Since $F(\epsilon,m,X_n)$ is insensitive to changes in m, the uniqueness with which $T_m(\epsilon,\lambda,\alpha)$ may be matched to a given set $\bar{N}$, X_n and m is determined mostly by the mathematical character of $p(\epsilon,m,X_n)$.

First, notice that p is positive for all X and ϵ when the refractive index is complex with a large absorption coefficient. The mathematical behavior of $p(\epsilon, X_n)$ for absorbing particles is so different from that due to dielectrics that equations 31 through 34 can be used to differentiate between the two even when observations are limited to a single wavelength. On the other hand, one cannot differentiate between various types of absorbing particles.

Secondly, note that measurements in the range $20^{\circ}<\epsilon<70^{\circ}$ cannot be used to determine the refractive index of dielectric or absorbing particles even when observations are available for several wavelengths.

Third, note that $p(X)$ is a very sensitive function of m at backscatter angles. Thus, observations should be made at several widely separated wavelengths at elongations, $140^{\circ}<\epsilon<180^{\circ}$. Observations in the range $20^{\circ}<\epsilon<70^{\circ}$ at one wavelength are nearly as valuable as those at several wavelengths.

Fourth, note that single wavelength measurements in the range $105^{\circ}<\epsilon<180^{\circ}$ can be used to determine whether the refractive index is high or low, and further, the size distribution as deduced from measurements in this region depends upon the refractive index. The burden in determining the unique size distribution rests in the range $20^{\circ}<\epsilon<70^{\circ}$ whereas the burden in determining the refractive index rests in the range $105^{\circ}<\epsilon<180^{\circ}$.

5. ELECTRONS

Equations 31 and 32 must be modified to account for electrons in the region $\epsilon > 20^{\circ}$. We assume that the number density of electrons is:

$$N_e(\rho) = N_e(R_o) \left[R_o/\rho \right]^{\beta} \tag{40}$$

The scattering from these electrons is given by:

$$dI_j(\theta,\lambda) = \frac{I_o \lambda^2}{8\pi^2 R^2} C(\lambda)\, N_e(\rho)\, \sigma_j\, dv \tag{41}$$

where $C(\lambda) = 4\pi^2 a_o^2/\lambda^2 \simeq 4 \times 10^{-23}/\lambda^2$ and σ_j is related to the Thompson scattering cross-section, i.e.:

$$\begin{aligned} \sigma_1 &= 1 \\ \sigma_2 &= \cos^2\theta \\ \sigma &= 1 + \cos^2\theta = 2 - \sin^2\theta \\ \Delta_e &= 1 - \cos^2\theta = \sin^2\theta \end{aligned} \tag{42}$$

Equations 31 and 32 become:

$$S = -\sum \bar{N}(R_o, X_n) F(\epsilon, m, X_n) - C(\lambda) N_e \left\{ \sigma(\epsilon) + E(\epsilon, \alpha, \beta) \right\} \tag{43}$$

$$T = -\sum \bar{N}(R_o, X_n)\, \Delta(\epsilon, m, X_n) - C(\lambda) N_e \left\{ \Delta_e(\epsilon) + G(\epsilon, \alpha, \beta) \right\} \tag{44}$$

where:

$$E(\epsilon, \alpha, \beta) = \frac{(\alpha-\beta)\cos^{\beta}\epsilon}{\sin^{\beta+1}\epsilon} \left[\frac{\beta+3}{\beta+2} \int_{\epsilon}^{\pi} \sin^{\beta}\theta d\theta - \frac{\sin^{\beta+1}\epsilon \cos\epsilon}{\beta+2} \right] \tag{45}$$

$$G(\epsilon, \alpha, \beta) = \frac{(\alpha-\beta)\cos^{\beta}\epsilon}{\sin^{\beta+1}\epsilon} \left[\frac{\beta+1}{\beta+2} \int_{\epsilon}^{\pi} \sin^{\beta}\theta d\theta + \frac{\sin^{\beta+1}\epsilon \cos\epsilon}{\beta+2} \right] \tag{46}$$

Both E and G can be evaluated quite easily for various assumed values of β and $\alpha-\beta$. The terms $\sigma(\epsilon) + E(\epsilon)$ and $\Delta_e(\epsilon) + G(\epsilon)$ can then be graphed and added as required to obtain a match between the pair S, T and the pair S_m, Tm given by equations 33 and 34.

It is well known that the relative angular scattering pattern due to electrons is exactly the same as that due to Rayliegh particles ($X \ll 0.1$).

Thus, if the electrons and Rayliegh particles exhibit the same decay constant $\alpha = \beta$, it is impossible to deduce N_e and $\overline{N}$ $(X<0.1)$ from scattering measurements at a single wavelength. One can also show that the electron density must be higher than the number density of Rayliegh particles by a factor of 10^{16} if the electron number density is to be determined from multi-color observations, i.e.:

$$N_e \geq 10^{16}\, \overline{N}(X<0.1) \tag{47}$$

This condition is fulfilled by 1 to 10 electrons per cm^3 in the Earth's vicinity.

Assuming that condition (47) is fulfilled we may investigate the color of the zodiacal light as it depends upon the relative number of large particles $(X>10)$ and electrons. Equations (43) and (44) may be differentiated with respect to λ and set equal to the observed color variation calculated by differentiating equations 33 and 34. Before doing so, note from the graphs in figures 5 and 3 that:

$$F(X) \simeq g(\epsilon)X^2 \quad \text{for } X>10 \text{ and } \epsilon>20^\circ$$

$$p(X) = \frac{\Delta}{F} \simeq f(\epsilon) \quad \text{for } X>10 \text{ and } \epsilon>90^\circ$$

where $g(\epsilon)$ and $f(\epsilon)$ are independent of λ. Thus, in the regions specified:

$$\frac{\partial F}{\partial \lambda} \simeq -2g(\epsilon)X^2/\lambda$$

$$\frac{\partial \Delta}{\partial \lambda} \simeq -\frac{2\Delta}{\lambda} \simeq -2f(\epsilon)g(\epsilon)X^2/\lambda$$

From equations (43) and (44) the contribution due to large particles $(X>10)$ and electrons is:

$$\frac{\partial S}{\partial \lambda} \simeq 2\sum_n \overline{N}(R_o, X_n)\, g(\epsilon)\frac{X_n^2}{\lambda} + \frac{C(\lambda)}{\lambda}\left\{\sigma(\epsilon)+E(\epsilon)\right\}N_e$$

$$\frac{\partial T}{\partial \lambda} \simeq 2\sum_n \overline{N}(R_o, X_n) f(\epsilon)g(\epsilon)\frac{X^2}{\lambda} + \frac{C(\lambda)}{\lambda}\left\{\Delta_e(\epsilon)+G(\epsilon)\right\}N_e$$

But X^2 and $C(\lambda)$ are proportional to λ^{-2}. So, for $X \gg 10$,

$$\frac{\partial S}{\partial \lambda} \simeq \frac{2}{\lambda^3} \left[\sum_n \bar{N}\,(R_o, X_n)(2\pi A_n)^2\, g(\epsilon) + 2\times10^{-23} N_e \left\{ \sigma(\epsilon) + E(\epsilon) \right\} \right] \quad (48)$$

$$\frac{\partial T}{\partial \lambda} \simeq \frac{2}{\lambda^3} \left[\sum_n \bar{N}\,(R_o, X_n)(2\pi A_n)^2\, g(\epsilon) f(\epsilon) + 2\times10^{-23} N_e \left\{ \sigma(\epsilon) + E(\epsilon) \right\} \right] \quad (49)$$

Thus, the electrons and large particles each contribute to the measured color variation in the region $20^\circ < \epsilon < 90^\circ$ in the same way. We cannot derive a similar formula in the range $\epsilon > 90^\circ$ because $p(X)$ depends on λ in this region.

Further discussion of the electron contribution will be delayed until specific observations are analyzed.

6. ACKNOWLEDGMENTS

This research was supported by the National Aeronautics and Space Administration under NASA Contract NASw-1206. The authors wish to thank Dr. Maurice Dubin for recommending financial support for the study and Dr. Bertram Donn for the use of many of his ideas as published previously with one of the authors (RSP).

7. REFERENCES

Divari, N. B. and Krylova, (1963), Soviet Astron. - AJ, 7, Translation of Ast. Zhur., 40, 1963.

Donn, B. and Powell, R. S., (1963), "Electromagnetic Scattering", Ed. by M. Kerker, Pergamon Press (London), 151-158.

Elsasser, H., (1963), Planetary Space Sci., 11.

Giese, H. R. and Siedentopf, H., (1962), Zeits. f. Astrophys., 54.

Huruhata, M., (1964) Tokyo Astronomical Observatory, Unpublished Manuscript.

Ingham, M. F., (1961), Mon. Not. Roy. Astron. Soc., 122.

Mie, Gustav (1908), Annalen der Physik, 25, No. 3.

Peterson, A. W. (1961), Astrophys. J., 133.

Powell, R. S. and Donn, B., (1966), To Be Published.

Robley, R., (1962), Ann. de Geophys., 18.

Weinberg, J. L. (1964), Report HIG-64-11, Hawaii Institute of Geophysics, University of Hawaii.